Emerging Prototype Sodium-Ion Full Cells with Nanostructured Electrode Materials

Wenhao Ren, Zixuan Zhu, Qinyou An, and Liqiang Mai**

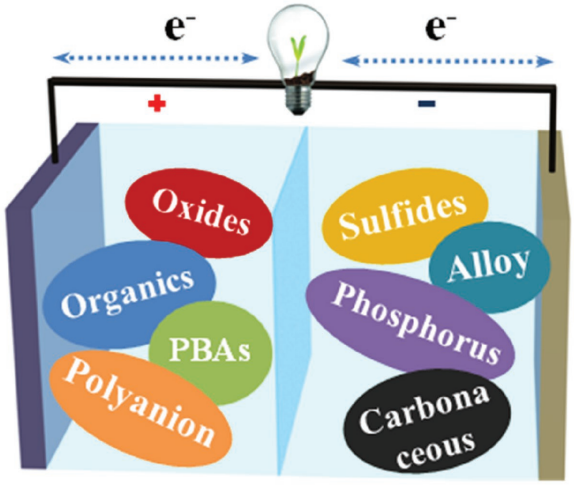

From the Contents

Due to steadily increasing energy consumption, the demand of renewable energy sources is more urgent than ever. Sodium-ion batteries (SIBs) have emerged as a cost-effective alternative because of the earth abundance of Na resources and their competitive electrochemical behaviors. Before practical application, it is essential to establish a bridge between the sodium half-cell and the commercial battery from a full cell perspective. An overview of the major challenges, most recent advances, and outlooks of non-aqueous and aqueous sodium-ion full cells (SIFCs) is presented. Considering the intimate relationship between SIFCs and electrode materials, including structure, composition and mutual matching principle, both the advance of various prototype SIFCs and the electrochemistry development of nanostructured electrode materials are reviewed. It is noted that a series of SIFCs combined with layered oxides and hard carbon are capable of providing a high specific gravimetric energy above 200 Wh kg^{-1}, and an $NaCrO_2$//hard carbon full cell is able to deliver a high rate capability over 100 C. To achieve industrialization of SIBs, more systematic work should focus on electrode construction, component compatibility, and battery technologies.

1. Introduction

Sustainable energy alternatives have become a global demand over the past decade due to ever-growing energy needs, increased consumption of fossil fuels, and environmental deterioration.[1–3] Lithium-ion batteries (LIBs) have achieved huge success since the first commercialization of an $LiCoO_2$//carbon cell in 1991. However, lithium abundance in the Earth's crust is relatively low, and the distribution of lithium sources mainly centers on South America, leading to a rise in the price of lithium, which seriously limits the development of LIBs.[4–8] As another effective energy storage device, sodium-ion batteries (SIBs) have attracted great attention owing to the large abundance and low cost of Na resources. Sodium, as the second-lightest and -smallest alkali metal with similar chemistry properties to that of lithium, has been considered as an ideal substitute to meet the demands for sustainable energy storage.[9–12] Surprisingly, earlier than the commercialization of LIBs, a few US and Japanese companies developed SIBs in full cell configurations, where a sodium–lead-alloy composite and P2-type Na_xCoO_2 were used, respectively, as a negative and a positive electrode in the 1980s.[13,14] Nevertheless, the energy density of SIBs, which is extremely important for applications, has been seriously restrained due to the heavier weight and high standard electrochemical potential of Na (0.33 V vs Li). Therefore, the essential challenges and opportunities for SIBs are as follows: 1) to develop SIBs that will maintain cycle life at a satisfactory rate, in a safe, affordable system, accompanied with a competitive energy density, in comparison with LIBs; 2) to establish a large-scale electrical grid,[15] where the operation cost of the SIBs is generally acceptable.

Energy density, power density, cycle life, and the cost of SIBs basically depend on the developments of electrode materials. Therefore, a large number of electrode materials (**Figure 1**a) have attracted great attention in sodium half-cells (sodium metal as the anode). For cathode materials, such as oxides, polyanion, hexacyanometalates, and organics, the most valuable innovation is to improve their energy density, which depends on three parameters; including specific discharge capacity (80–200 mAh g^{-1}), average operating voltage (2.5–4 V), and tap density (0.6–2.8 g cm^{-3}).[16] The specific discharge capacity and average operating voltage determine the specific gravimetric energy of the battery, while the tap density mainly influences the specific volumetric energy. For anode materials, including carbonaceous, metal oxide/sulfide, alloy, and phosphorus, specific capacities of 100–2000 mAh g^{-1} and average operating potentials of 0.1–2 V can be obtained in a sodium half-cell. The major challenge for anode materials is to increase their initial Coulombic efficiency (CE) and cycling stability. Low initial CE and poor cycling stability consumes the active sodium ions in a full cell (free from metallic sodium).[17] In addition, the presodiation method, which has been extensively used to offset the consumption of Na ions during the solid electrolyte interface (SEI) formation, still retains a series of limitations, and has a long way to go before practical application.

Notably, despite that the investigation of sodium-ion full cells (SIFCs) is in the early stages, the successful optimization

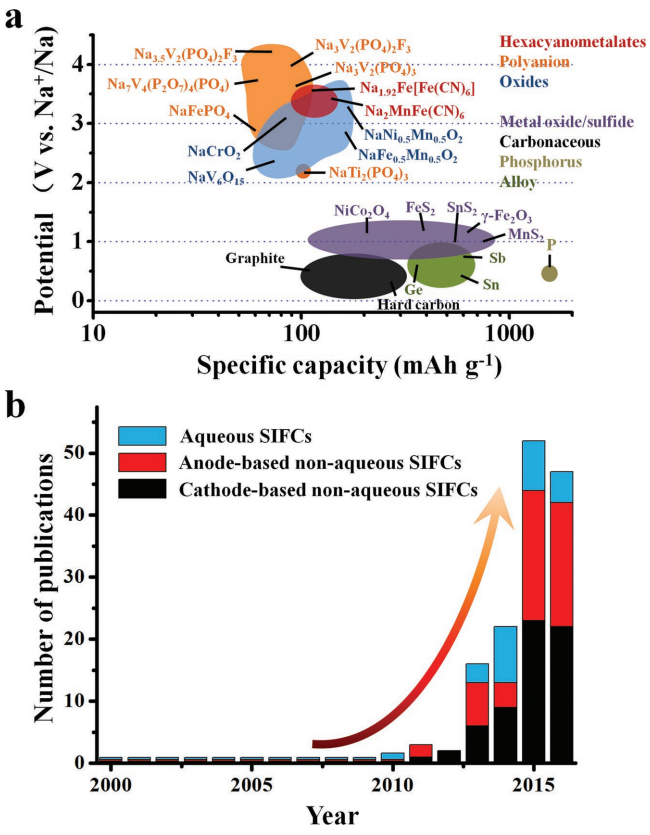

Figure 1. a) Capacity–voltage diagrams of representative cathode and anode electrode materials. b) The number of publications on SIFCs to December 2016.

of electrode materials and sodium half-cell lays a solid foundation for the development of full cells, and the scientific research regarding SIFCs is in a great boom since 2010 (Figure 1b). Particularly, some remarkable progress of SIFCs has been briefly summarized below. For cathode-based non-aqueous SIFCs, an $Na[Ni_{0.60}Co_{0.05}Mn_{0.35}]O_2$//hard-carbon[18] exhibited a high specific capacity of 157 mAh g^{-1} at 0.1C, and still remained 80% of the capacity after 300 cycles. An Na-enriched '$Na_{3.5}V_2(PO_4)_2F_3$'-based full cell[19] showed a high output voltage of 3.5 V, with an enhanced specific capacity of 110 mAh g^{-1}. While for anode-based non-aqueous SIFCs, $Na_2Ti_3O_7$//$Na_{2/3}(Ni_{1/3}Mn_{2/3})O_2$[20] was capable of delivering a discharge capacity of 110 mAh g^{-1} at a high rate of 2 C, and retained a capacity of 147 mAh g^{-1} at 0.5 C over 100 cycles. The $Na_{2/3}Ni_{1/3}Mn_{2/3}O_2$//Sb[21] was discovered to have a

W. Ren, Z. Zhu, Prof. Q. An, Prof. L. Mai
State Key Laboratory of Advanced Technology for Materials Synthesis and Processing
Wuhan University of Technology
Wuhan 430070, China
E-mail: anqinyou@whut.edu.cn; mlq518@whut.edu.cn
Dr. L. Mai
Department of Chemistry
University of California Berkeley
Berkeley, CA 94720, USA

DOI: 10.1002/smll.201604181

high discharge capacity of 620 mAh g^{-1} and a superior rate capability (200 mAh g^{-1} at 20 A g^{-1}). As for aqueous SIFCs, classical $Na_{0.44}MnO_2$//$NaTi_2(PO_4)_3$[22] displayed a specific capacity of 20 mAh g^{-1} at an ultrahigh rate of 270 C, with promoted cycling performance.

Although several excellent reviews have introduced electrochemistry,[23] cathode materials,[16,24–27] anode materials,[17,28,29] electrolyte,[30] and also the development of SIBs,[10,31,32] no review has specially focused on and summarized sodium-ion full cells, which play an important role in bridging the sodium half-cell and commercial batteries. In this contribution, this Review principally summarizes the most recent discoveries, technological developments, and major challenges of electrode-based SIFCs. Since the electrochemical performance of SIFCs is tightly related to the cathode/anode, including structure, composition and mutual matching relationship, this Review focuses on the advance of various prototype full cells, and the strategies of enhancing their electrochemical behaviors with regard to electrode modification and electrochemistry considerations. This Review opens the door to accelerating the development and application of high-performance SIBs.

Wenhao Ren received his B.S. degree in the Department of Materials Science and Engineering from Wuhan University of Science and Technology (WUST) in 2012 and he is currently working toward a Ph.D. degree in Material Science at Wuhan University of Technology (WUT). His current research involves nanomaterials and devices for energy storage.

Qinyou An is Associate Professor of Materials Science and Engineering at WUT. He received his Ph.D. degree from WUT in 2014. He carried out his postdoctoral research in the laboratory of Prof. Yan Yao at the University of Houston in 2014–2015. Currently, his research interest includes energy-storage materials and devices.

Liqiang Mai is Chair Professor of Materials Science and Engineering at WUT. He received his Ph.D. from WUT in 2004. He carried out his postdoctoral research in the laboratory of Prof. Zhonglin Wang at Georgia Institute of Technology in 2006–2007 and worked as an advanced research scholar in the laboratory of Prof. Charles M. Lieber at Harvard University in 2008–2011. His current research interests focus on nanowire materials and devices for energy storage.

2. Insights in SIFCs

2.1. Full Cell Configurations

Figure 2a shows the basic working principle of an SIFC, which contains a $NaMnO_2$ cathode, hard-carbon (HC) anode, separator film, and electrolyte. The overall chemical reaction is based on a reversible intercalation/deintercalation processes of Na ions between two electrodes. Systems, components, structures, and operating mechanisms of SIFCs are essentially the same with LIBs, except the replacement of sodium ions.[33,34] During the charge process, an oxidation reaction takes place at the cathode, with Na ions extracting from lattice sites accompanied by electrons that move from cathode to anode via an external circuit to achieve charge balance. Conversely, Na ions extract from the anode and come back to the cathode lattice sites for the discharge process. There also exist a series of device configurations for the full cells, such as coin-cell (Figure 2b), cylindrical battery (Figure 2c), and aluminium-pouch cell (Figure 2d). The coin-cell devices are extensively used as a facile configuration for scientific research and small equipment applications, including electronic scale, calculator, watch, etc. According to its diameter and thickness, it can be divided into CR 1220, CR 2025, CR 2430, CR 3032, and so on. As another type of full cell, cylindrical battery, especially model 18650, is recognized as a high energy, low cost, and easily modularized power source. It is assembled by winding craft to make full use of the space and realize the close contact of the electrode. The external packing of the battery consists of a steel shell containing a safety vent. In recent years, the model-18650 LIBs have been extensively used in the charging of treasures, laptops, electric torches, model airplanes, etc. The detailed technological processes for the fabrication of 18650 cells are shown in **Figure 3**. In order to further improve the energy density and safety performance of the battery, a pouch cell, fabricated by a zigzag stacking technique, packaging with an Al-plastic film has been developed. Compared with a metal-case-based battery, the lighter Al-plastic film enables the battery to obtain a higher gravimetric energy density (≈10%) and avoid explosion danger.[3] The zigzag stacking technique, which creates a parallel circuit among electrodes, could dramatically decrease the resistance of the battery, resulting in high power durability. Although the pouch cell is troubled by relatively high cost, its applications in high-end electronic products has increased, including in mobile phones, tablet devices, electric vehicles, etc.

2.2. Mass and Cost Composition Assessments

The composition assessments of model-18650 SIFCs in terms of mass and cost ratio have been illustrated. The assessments are based on the most promising layered oxide cathode coupled with a hard carbon anode. A 1 M $NaPF_6$ in an organic

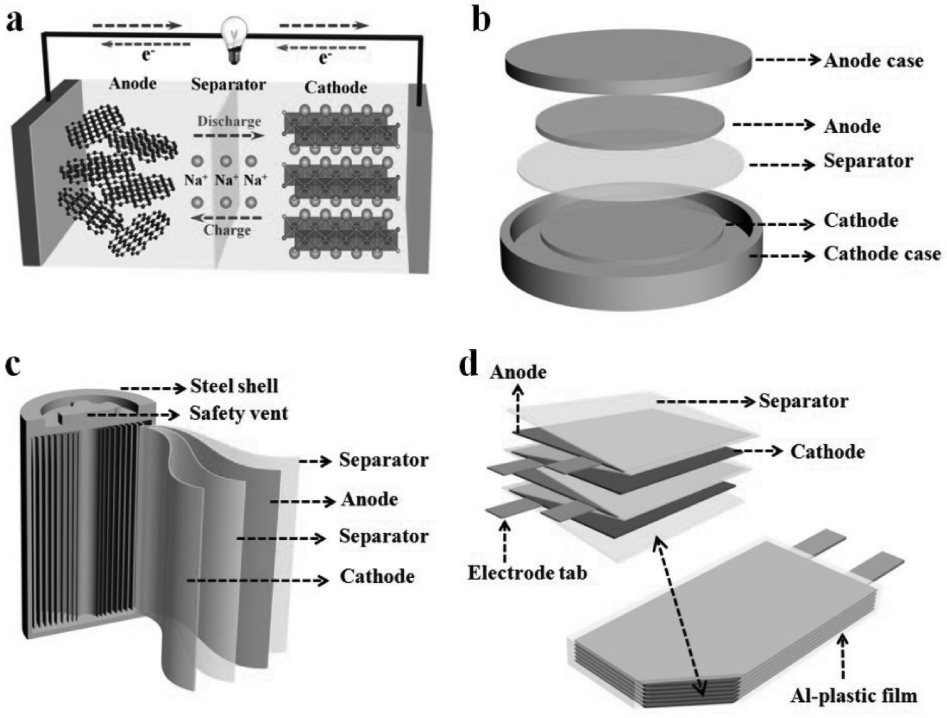

Figure 2. a) Working principle of the sodium-ion full cells ($NaMnO_2$ vs hard carbon). Device configurations of b) coin cell, c) cylindrical battery, and d) pouch cell.

solvent is used as an electrolyte. The auxiliary materials selected here are consistent with LIBs, including oil-based N-methyl-2-pyrrolidone (NMP, solvent), polyvinylidene fluoride (PVDF, binder) of the cathode, and water-based deionized water (solvent), carboxymethylcellulose (CMC, binder), and styrene-butadiene rubber (SBR, stabilizer) of

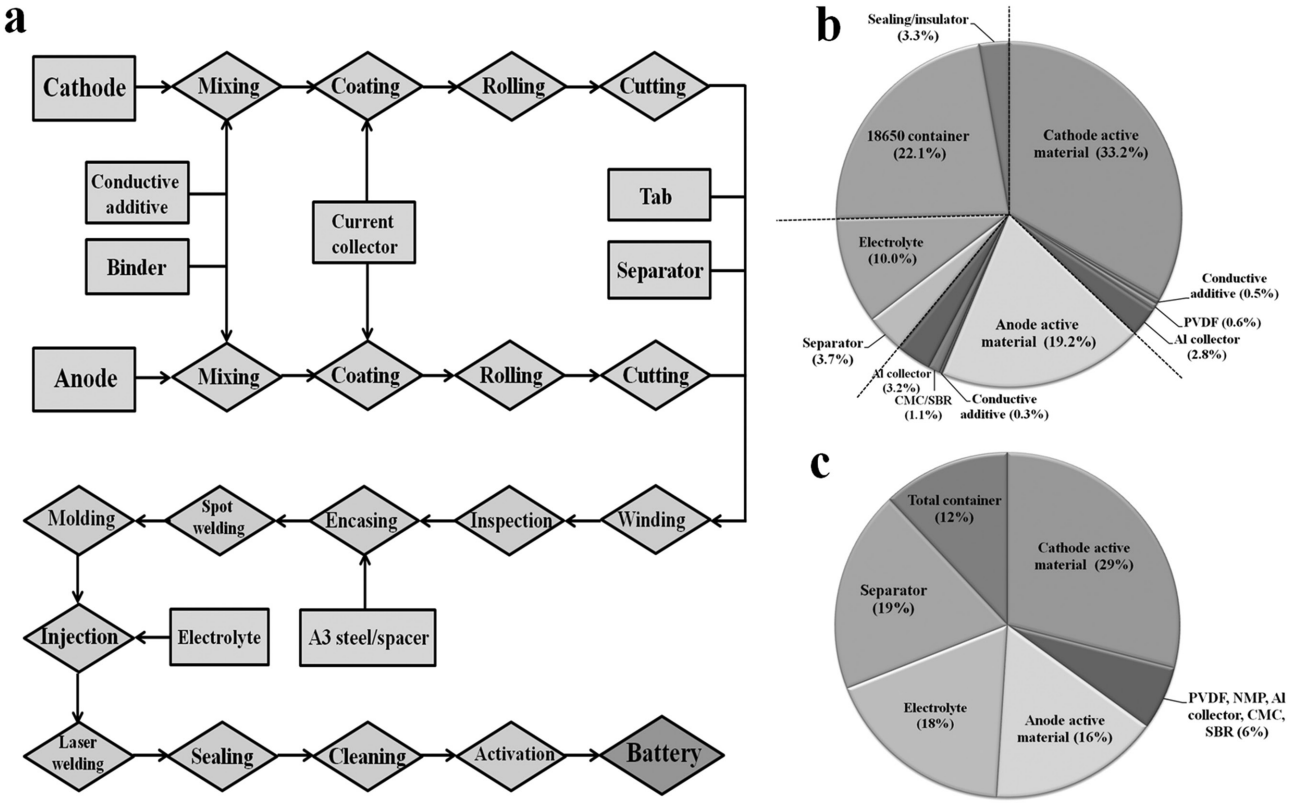

Figure 3. a) The detailed technological processes for the fabrication of 18650 cells. b) Mass- and c) cost-composition forecast in model 18650 SIFCs.

the anode. Notably, Al instead of Cu is utilized as the current collector for both the cathode and anode, since no alloy reaction occurs with sodium at a low potential. The substitution of much lighter Al is able to reduce the total weight of battery, thus the other components exhibit a higher share in comparison with LIBs (Figure 3b).[35] The cell housing of 18650 possesses a relatively higher proportion, which decreases the specific gravimetric energy. The utilization of an Al-plastic film to the pouch cell has been considered as a valid approach to reduce package weight. The calculation of cost composition in Figure 3c is based on the current price of raw materials without labor cost, R&D expenses, and operating cost. Obviously, the cost ratio of cathode active material in SIFCs is 29%, which is much smaller than that of in LIBs (≈40%). Besides, the total cost of SIFCs can be further reduced owing to the replacement of copper. Since the development of SIFCs is in the initial state, the expense of electrolyte and separator may occupy a higher proportion that follows the development trend of LIBs.

2.3. Contribution of Capacity

Considering the great significance of specific capacity and energy density in SIFCs, the relationship between tthe wo of them, regarding cathode/anode materials at various operating voltages, is calculated.[36,37] For cathode materials (**Figure 4**a), the specific capacity is almost in a linear relation with the energy density of the full cell, where the full cell (3 V) delivers 225, 265, 300, 332, and 360 Wh kg^{-1} at 100, 125, 150, 175, and 200 mAh g^{-1}, respectively, indicating the profound significance of improving the specific capacity of the cathode. For anode materials, the enhancement of specific capacity exhibits a moderate effect with respect to energy density. As observed in Figure 4b, the energy density of the full cell (3 V) increased from 300 to 360 Wh kg^{-1} as the specific capacity of anode doubled from 300 to 600 mAh g^{-1}. The yield rate for energy density declines further, accompanied by the promotion of specific capacity above 1000 mAh g^{-1}. In addition, the high specific capacity of the anode is basically associated with high mass loading of the cathode in the full cell assembly, which may result in inferior rate performance of the cathode.

Capacity, power, and lifetime have been considered as the uppermost important indexes in battery application. Correspondingly, researchers pay much attention in terms of specific capacity, rate capability, and cycle life of the electrode materials. In general, these parameters of the electrode are investigated separately, and there is no direct connection between the three of them. However, the capacity does have significant influence to the power and lifetime in practical application. According to Equation (1), the lifetime (T_s) is proportional to the capacity (C_a) if the cycle number (N) and output current (I_A) of battery are constant. Taking a cell phone as an example, the improved capacity is able to prolong the working hour per cycle, and thus total lifetime of

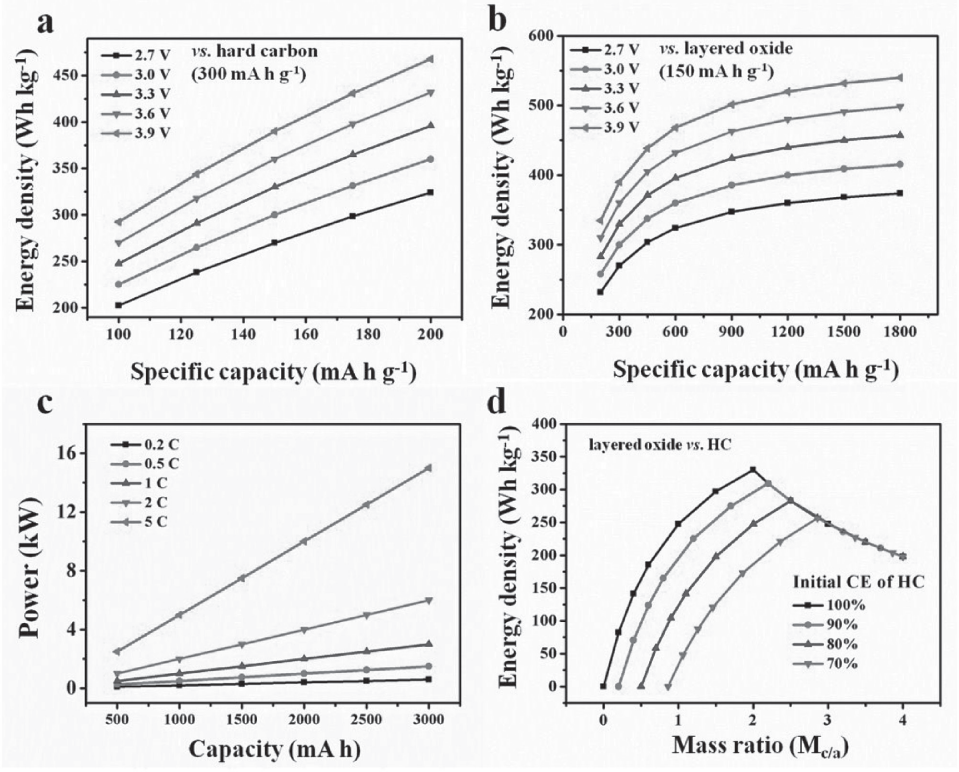

Figure 4. The specific gravimetric energy of full cells based on the specific capacity of a) cathode and b) anode at various average operating voltages from 2.7 to 3.9 V (without regard to initial CE). c) The capacity–power curves of the full cells (3.3 V) at different C-rate. d) The relationship of energy density and $M_{c/a}$ in the full cell (3.3 V).

the battery. In Equation (2), the output power (P) exhibits a linear relationship with capacity (C_a) based on the constant operating voltage (U) and rate (R). It is observed (Figure 4c) that the power of the battery increased from 2.5 to 15 kW as the capacity range from 500 to 3000 mAh, indicating the greater contribution of capacity in a high rate condition.

$$T_S = \frac{N * C_a}{I_A} \tag{1}$$

$$P = U * R * C_a \tag{2}$$

2.4. Nanostructured Electrode Materials

Nanostructure construction strategies have been extensively applied to promote the holistic electrochemical properties of electrode materials, since nanomaterials that vary from zero-dimensional (0D) to three-dimensional (3D) display a series of advantages towards the bulk materials.[10] 0D nanomaterials represent nanoparticles with diameters from several nanometers to one hundred nanometers. The nano-miniaturization of particle size can not only increase the activity of materials, but also improve the kinetics of electrochemical reactions. The diffusion rate of Na ions in nanoparticles can also be effectively improved through multi-dimensional intercalation process.[23] Besides, the construction of porous or hollow structure in 0D nanomaterials is able to further decrease the diffusion pathway of Na ions and enhance the adaptability of volume expansion. One-dimensional (1D) nanomaterials, typically the nanowires, gained much attention in the fields of electrode materials and devices, owing to their rapid charge transport in the crystal growth direction. The rate capability of 1D nanomaterials is governed by improved kinetics of nanowires, together with the short ionic diffusion distance in the axial direction. However, the cycling stability of the pure nanowires is generally faded due to an irreversible structural change during the deep insertion/deinsertion of Na ions. To improve the structural stability, core–shell nanowires or nanowire arrays are developed to accommodate the stress-strain during charge/discharge. Two-dimensional (2D) nanomaterials with layered structure, such as transition metal oxides, metal chalcogenides, and other 2D composites, have achieved considerable interest. It exhibits outstanding Na storage properties owing to their excellent electronic conductivity and large surface area. The continuous electron transport in two dimensions can dramatically promote the electrochemical kinetics of the materials, and the enlarged surface area allows for rapid ionic diffusion. Different from low-dimensional nanomaterials, 3D nanomaterials are able to provide a framework structure, which dramatically enhances the structural stability of the material and improves the electrical transport properties. In brief, with the developments of nano-functionalization, both the cathode and anode materials have shown significant improvements in electrochemical properties.[16,17] It is, however, necessary to take tap density, synthesis technologies, as well as cost into consideration when entering industrialization.

2.5. Matching Principle of Electrode Materials

Compared with sodium half-cell, the amount of Na ions in the full cell is fixed, and no extra Na ions can compensate the capacity lost during undesirable side reactions and irreversible intercalation/deintercalation processes. Thus, in order to establish a preferable battery system and take full advantages of electrode materials, the capacity matching of the cathode and anode electrode should be carefully controlled.[38] There is a great difference between practical-battery and lab-battery regarding the matching of electrode materials. In practical applications, the battery with high specific volumetric energy and high power density is the major pursuit. Thus, the mass ratio of cathode and anode has been strictly controlled to achieve the battery balance. In the laboratory, researchers mainly focus on the specific gravimetric energy of the active materials, and the calculation of the capacity is always based on one side (mass of cathode or anode active material). In order to measure the performance of the targeted electrode material, the matching principle of SIFCs is based on the use of excess counter electrode. Taking $Na[Ni_{0.25}Fe_{0.25}Mn_{0.5}]O_2$// hard-carbon full cell as an example, if the target electrode is a cathode (cathode-based), the presodiation of the hard carbon should be performed to realize normal operation of the $Na[Ni_{0.25}Fe_{0.25}Mn_{0.5}]O_2$ material. On the opposite (anode-based), the overload of $Na[Ni_{0.25}Fe_{0.25}Mn_{0.5}]O_2$ is necessary, which aims to compensate the Na ions lost due to SEI formation and an irreversible reaction. The matching principle of electrode materials in a lab-battery may mislead the readers regarding the understanding of the battery assembly in practical application. Therefore, the energy-density–mass-ratio curve of the layered oxide//HC full cell with respect to total mass of active material has been calculated (Figure 4d). The full cell with low mass ratio of cathode to anode ($M_{c/a}$) is cathode-limited, while the one with high $M_{c/a}$ is anode-limited. The maximum energy densities of the full cells vary from 256 to 330 Wh kg^{-1} when the initial CE of the HC increased from 70 to 100%. In brief, the excess of anode or cathode material would lower the specific gravimetric energy of the full cell, and the initial CE of anode material plays an important role in the full cell assembly.

3. Non-Aqueous Cathode-Based SIFCs

Since the energy gap between the lowest unoccupied molecular orbital (LUMO) and the highest occupied molecular orbital (HOMO) of electrolyte components determine the theoretical upper limit of the electrochemical stability window of battery,[6,39] non-aqueous SIFCs have gained great attention due to the high operating potential. As the electrochemical performance of SIFCs in terms of specific energy, specific power, and cycle life is closely related to cathode materials, the investigation of non-aqueous SIFCs with regard to cathode materials has become the major target, including oxides, polyanionic compounds, hexacyanometalates, and organics.

3.1. Oxides-Based SIFCs

The initial report of layered oxide materials in SIBs can be traced back to 1980s for the purpose of investigating post-LIB systems with low cost and high energy density. More recently, a series of layered oxides ($NaMO_2$, M = Cr, Co, Fe, Ti, V, Mn, Ni, and a mixture of 2 or 3 elements) have been explored as SIFCs cathode due to their simple structures, high capacities, and ease of synthesis.[16,24] Typical Na layered oxides can be defined as P2- (prismatic) and O3- (octahedral) phases based on the surrounding Na environment and the number of unique oxide layer packing. The number indicates the repeated transition metal layers within a unit cell, and the letter indicates the environment where Na is located; for example, ABCABC in O3, ABBA in P2, and ABBCCA in P3.[40]

3.1.1. Single-Metal Oxides

Na_xCoO_2 has been considered as a promising cathode for SIFCs owing to the success of its counterpart $LiCoO_2$.[41] However, Na_xCoO_2 has revealed surprising differences in full cells with respect to analogue lithium-based materials, and does not show attractive charge/discharge performance due to the larger radius of the Na^+.[42,43] A novel, high-power SIFC assembled by a layered P2-$Na_{0.7}CoO_2$ cathode coupled with a graphite anode in an optimized ether-based electrolyte, was firstly addressed by Scrosati's group.[44] Prior to assembling the full cell, the graphite anode has been electrochemically activated in sodium half-cells in order to remove its small irreversible capacity and achieve a partial sodium intercalation for compensation of the sodium deficiency of the cathode used without pre-cycling. The cell represents an original sodium rocking-chair battery, obtained by combining the intercalation/deintercalation processes of sodium within the cathode and anode layers, which delivers a reversible capacity of about 80 mAh g^{-1} (0.5–3.7 V) over 100 cycles. Moreover, the capacity retention of the full cell cycled at 10 C reaches as high as 80% after 1200 cycles, indicating the outstanding stability of the full cell.

A great number of research regarding rechargeable Na-ion batteries have been focused on manganese-based oxides owing to their large-size tunnels for Na^+ insertion/extraction.[45,46] However, the layered and tunnel-type manganese oxides always suffer from poor cycling stability, which is attributed to the inability to accommodate Jahn–Teller distortion following the reduction of Mn (IV) to Mn (III) within the rigid, close-packed, oxide-ion structures.[47] Nanomaterials and nanotechnology have offered a new approach to improve the structure and properties of well-established materials for energy applications. Cao et al.[48] reported the synthesis of single crystalline $Na_4Mn_9O_{18}$ ($Na_{0.44}MnO_2$) nanowires with a high reversible capacity and exceptional cycling performance as an SIBs cathode. The $Na_4Mn_9O_{18}$-nanowire electrode material, after calcination at 750 °C, delivers a reversible capacity of 128 mAh g^{-1} at 0.1 C, with excellent capacity retention capability of 77%, even after 1000 cycles at 0.5 C. The SIFCs based on the as-prepared $Na_4Mn_9O_{18}$ nanowires as a cathode, combined with pyrolyzed carbon as the anode, are also presented, which maintains 73% of initial capacity after 100 cycles with an average discharge voltage of 2.7 V.

$NaCrO_2$ was initially confirmed by the viability of using as the Na^+ extraction/insertion electrode in 1982 by Hagenmuller et al.[49] Recently, a O3-type layered $NaCrO_2$[50] as the Na^+ host structure was revisited due to its larger interslab distance in comparison with $LiCrO_2$, which is electrochemically inactive in LIBs.[51] As for full cell investigation, Yu et al.[52] reported the layered O3-type $NaCrO_2$ material as the cathode in SIFCs, which is synthesized via an emulsion-drying method. Notably, SIFCs using $NaCrO_2$ as a cathode and hard carbon as an anode are fabricated in a pouch-cell configuration. Thermal stability of $NaCrO_2$ has been investigated through in situ high temperature XRD (**Figure 5**a) and differential scanning calorimetric (DSC) measurements. Even after a high exothermic reaction at 400 °C, the weight loss of C-$Na_{0.5}CrO_2$ is quite small owing to the effective carbon-coating layer, and the lower evolution of oxygen from the crystal structure is likely to retard phase segregation. The initial specific capacity of the full cell reaches up to 102 mAh g^{-1} (Figure 5b), and a superior rate capability is obtained even at a high rate of 100 C (10 A g^{-1}), which demonstrates a great potential for high-power applications. Also, other single-metal layered oxides such as $Na_4Mn_9O_{18}$,[48] $Na_{2.55}V_6O_{16}{\cdot}0.6H_2O$,[53] Na_2NiO_2,[54] and $Na_{1.25}V_3O_8$[55] have also been explored.

3.1.2. Binary-Metal Oxides

Based on the different electrochemistry characteristics of various single-metal oxides, such as the good ionic diffusivity of Na_xCoO_2,[56] the high specific capacity of Na_xMnO_2,[57] and low cost of $NaFeO_2$,[58] the investigation towards synergistic effects of different metals has become a promising strategy to improve electrochemical performance. As for binary-metal-oxides-based SIFCs, Chen and co-workers[59] reported a P2-$Na_{0.6}[Cr_{0.6}Ti_{0.4}]O_2$ layered oxide, which is completely Na^+/vacancy-disordered at any sodium content. This cation-disordered material can function as both positive and negative electrodes, with average operation voltages of 3.5 and 0.8 V, corresponding to the redox couples of Cr^{3+}/Cr^{4+} and Ti^{3+}/Ti^{4+}, respectively. A symmetric SIFC using P2-$Na_{0.6}[Cr_{0.6}Ti_{0.4}]O_2$ as both negative and positive electrodes exhibits an average voltage plateau at 2.53 V, with excellent rate and cycling performance. As another promising binary-metal oxide, O3-type layered $Na_{0.8}Ni_{0.4}Ti_{0.6}O_2$, containing two electrochemically-active transition metals with redox couples of Ni^{4+}/Ni^{2+} and Ti^{4+}/Ti^{3+} has been reported (Figure 5c).[60] The polarization and irreversibility effect of $Na_{0.8}Ni_{0.4}Ti_{0.6}O_2$-symmetric SIFC in the first charge and discharge process have been successfully suppressed through pre-desodiated and presodiated method. A reversible discharge capacity of 85 mAh g^{-1} can be obtained in the first cycle with an output voltage of 2.8 V. Yuan et al.[61] reported the novel honeycomb-ordered O3-$Na_3Ni_2SbO_6$, and the cathode delivers a discharge capacity of 110, 106, 104, and 100 mAh g^{-1} at current rates of 1 C, 5 C, 10 C, and 20 C, respectively. Even at a high rate of 30 C (6000 mA g^{-1}), the reversible capacity still reaches to 90 mAh g^{-1}. When coupled with Sb/C anode, the SIFC shows

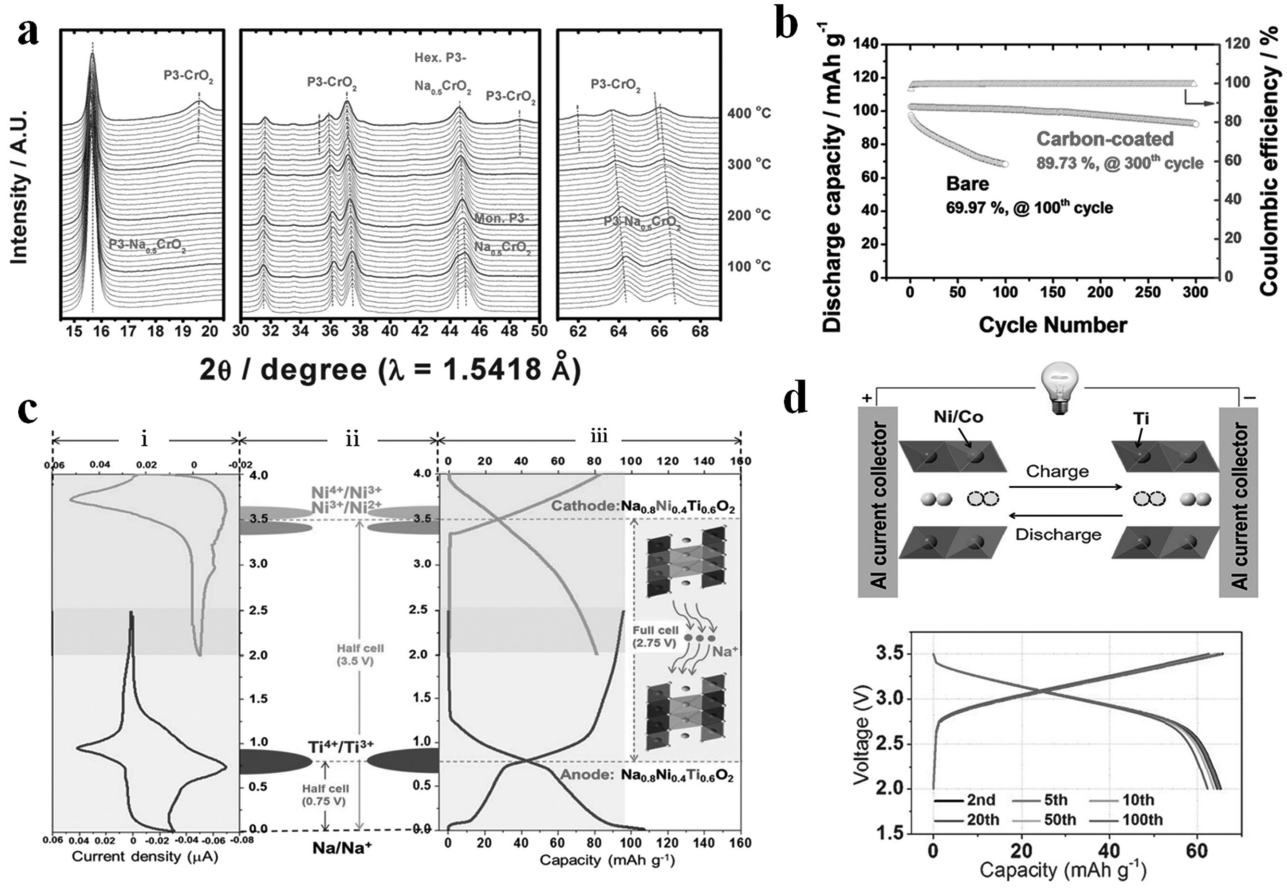

Figure 5. a) In situ high-temperature XRD patterns of electrochemically de-sodiated C-$Na_{0.5}CrO_2$. b) First charge and discharge cycles of bare and C–$NaCrO_2$ at 20 mA g^{-1} from 1.8 to 3.4 V at 25 °C. Reproduced with permission.[52] Copyright 2015, Royal Society of Chemistry. c) The electrochemical performance of O3-type $Na_{0.8}Ni_{0.4}Ti_{0.6}O_2$ in the half-cell. The inset shows the predicted average voltage of 2.8 V in the bipolar, $Na_{0.8}Ni_{0.4}Ti_{0.6}O_2$-based symmetric cells. Reproduced with permission.[60] Copyright 2015, Royal Society of Chemistry. d) A diagram of the proposed symmetric cell based on P2-$Na_{0.66}Ni_{0.17}Co_{0.17}Ti_{0.66}O_2$ (upside). The charge/discharge profiles of the 2nd, 5th, 10th, 20th, 50th, and 100th cycles with a rate of 1C (underside). Reproduced with permission.[66] Copyright 2015, Wiley–VCH.

a discharge voltage of 2.4 V, and delivers an initial capacity of 100 mAh g^{-1}. The full cell remains 70% of its initial capacity after 50 cycles at a current density of 0.1 C, which needs further promotion.

Owing to the earth-abundant Mn resources and the relatively high operating voltage of the $Ni^{2+/3+/4+}$ redox reaction, $NaNi_{0.5}Mn_{0.5}O_2$ becomes another interesting host material for SIFCs. Aurbach's group[62] reported the Na-ion and Li-ion full cells based on $NaNi_{0.5}Mn_{0.5}O_2$ and $LiNi_{0.5}Mn_{0.5}O_2$ cathodes, and hard-carbon anode. On the one hand, the surface films resistance of hard-carbon electrodes in Na cells is much higher than in Li cells, due to the slower Na ions diffusion within surface films comprising ionic sodium compounds. On the other hand, the diffusion of Na ions in the $Na_x[NiMn]O_2$ host is faster than Li-ions diffusion in $Li_x[NiMn]O_2$, resulting in the better rate capability of sodium-ions intercalation cathodes than the similar lithium-ion electrodes. Other $NaNi_{0.5}Mn_{0.5}O_2$-based SIFCs associated with SnC as the anode have also been investigated.[63] The presodiation of the Sn-C composite anode is performed in order to reduce its initial irreversible capacity, and the battery balance is achieved through controlling the cathode/anode ratio to 1:2. The Sn-C//$NaClO_4$ PC-FEC//$Na(Ni_{0.5}Mn_{0.5})O_2$ full cell is able to deliver a maximum energy density of 300 Wh kg^{-1}.

3.1.3. Tenary-Metal Oxides

Based on the successful application of $LiNi_xCo_yMn_zO_2$ and $LiNi_xCo_yAl_zO_2$ in LIBs, ternary-metal layered oxides in SIBs have also attracted numerous attention.[64,65] Sun and co-workers[18] reported a radially-aligned, hierarchical columnar structure with varied chemical composition from the inner end ($Na[Ni_{0.75}Co_{0.02}Mn_{0.23}]O_2$) to the outer end ($Na[Ni_{0.58}Co_{0.06}Mn_{0.36}]O_2$). When tested as a full cell with a hard-carbon anode, this cathode material exhibited a capacity retention of 80% (125 mAh g^{-1}) during 300 cycles, and a high rate capability of 134 mAh g^{-1} at 5 C. The temperature adaptability of the full cell has also been explored; it delivered capacities of 143, 147.6, and 128.8 mAh g^{-1} at 30, 55, and 0 °C, respectively. Even at a low temperature of -20 °C, it still maintained a capacity of 114 mAh g^{-1}, indicating powerful competitiveness compared with LIBs. Guo et al.[66] reported a bipolar electrode material P2-$Na_{0.66}Ni_{0.17}Co_{0.17}Ti_{0.66}O_2$ synthesized through a simple solid-state reaction, which not only exhibited a remarkable high output potential of about 3.74 V

in the cathode side, but also delivered a very safe voltage of 0.69 V at the anode side (Figure 5d). This symmetric P2-$Na_{0.66}Ni_{0.17}Co_{0.17}Ti_{0.66}O_2$ SIFC shows the superior high operating voltage of 3.1 V and the prolonged cycle-life of 1000 cycles, as well as performing with a specific capacity of 92 mAh g^{-1} and excellent rate capability (about 65 mAh g^{-1} at a rate of 2 C), indicating powerful competitiveness in comparison with previously reported symmetric SIFCs. Huang's group[67] reported a Co/Ni free and air-stable layered oxide of O3-$Na_{0.9}[Cu_{0.22}Fe_{0.30}Mn_{0.48}]O_2$ via a simple solid-state reaction. When used as sodium half-cell cathode, the O3-$Na_{0.9}[Cu_{0.22}Fe_{0.30}Mn_{0.48}]O_2$ exhibited a discharge capacity of 98 mAh g^{-1}, and the capacity retention is as high as 97% after 100 cycles. When tested as a $Na_{0.9}[Cu_{0.22}Fe_{0.30}Mn_{0.48}]O_2$//hard-carbon SIFC, the full cell showed a high average voltage of 3.2 V at 0.5 C. The investigation of SIFCs with other configuration such as pouch cell is of great importance. A 1 Ah soft-packed battery using large-scale synthesized $NaNi_{1/3}Fe_{1/3}Mn_{1/3}O_2$ cathode and hard-carbon anode has been produced.[68] The fabricated 1 Ah soft-packed battery exhibits good cycling stability, and the capacity still remains at 0.73 Ah after 500 cycles at 1 C. The crystal structural evolution of $Na_xNi_{1/3}Fe_{1/3}Mn_{1/3}O_2$ during charge/discharge process has been studied through ex situ XRD experiments, and the layered crystallographic structure of the $Na_xNi_{1/3}Fe_{1/3}Mn_{1/3}O_2$ cathode remained stable after 500 cycles. This work demonstrates the great potential of the $Na_xNi_{1/3}Fe_{1/3}Mn_{1/3}O_2$ cathode for advanced SIFCs. Also, other ternary-metal-oxides-based SIFCs have also been explored, such as $NaNi_{1/3}Fe_{1/3}Mn_{1/3}O_2$// HC,[69] $Na[Ni_{0.25}Fe_{0.5}Mn_{0.25}]O_2$//$Fe_3O_4$,[70] $Na_{7/9}Cu_{2/9}Fe_{1/9}Mn_{2/3}O_2$// HC,[71] $Na_{0.9}[Ni_{0.4}Mn_xTi_{0.6-x}]O_2$//HC,[72] etc.

Notably, ionic substitution is an valid strategy in promoting energy density and cycling stability.[73,74] O3-type Li-containing multi-metal oxides obtained by electrochemical Li–Na ion exchange from Li-rich layered oxides have been considered to possess the promising characteristic of high capacity.[75,76] Liu et al.[77] reported a new O3-$Na_{0.78}Li_{0.18}Ni_{0.25}Mn_{0.583}O_w$ material by electrochemical Li–Na ion exchange from $Li_{1.167}Ni_{0.25}Mn_{0.583}O_2$, and the cathode exhibits exceptionally high specific capacity of 240 mAh g^{-1} in the voltage range of 1.5–4.5 V, indicating the energy density reaches up to 675 Wh kg^{-1}. Even evaluated as $Na_{0.78}Li_{0.18}Ni_{0.25}Mn_{0.583}O_w$//$SnS_2$-rGO SIFC, it still delivers a high energy density of ≈400 Wh kg^{-1}, suggesting a great potential for high-energy applications. In addition, the substitution of transition metals by Li has been considered as a way to stabilize the crystal structure during the charge and discharge process.[78,79] Sun and co-workers[80] reported a layered $Na[Li_{0.05}(Ni_{0.25}Fe_{0.25}Mn_{0.5})_{0.95}]O_2$ cathode that was synthesized through a coprecipitation approach. The layered $Na[Li_{0.05}(Ni_{0.25}Fe_{0.25}Mn_{0.5})_{0.95}]O_2$ cathode showed an ultra-high specific capacity of 180.1 mAh g^{-1} at 0.1 C, as well as outstanding rate capability (1 C: 130.9 mAh g^{-1}, 5 C: 96.2 mAh g^{-1}), which was attributed to the excellent structural stability by the introduction of Li into the transition metal layer. Furthermore, the $Na[Li_{0.05}(Ni_{0.25}Fe_{0.25}Mn_{0.5})_{0.95}]O_2$// hard-carbon full cell displays a high discharge capacity of 177 mAh g^{-1} at 0.1 C, and exhibits a superior capacity retention of 76% after 200 cycles at 0.5 C, with an average voltage of 3.3 V.

In short, layered-oxides-based SIFCs are revealed to provide the most attractive specific discharge capacity with various charge and discharge properties. However, they suffers from relatively poor cycling stability during the deep insertion/deinsertion of Na ions. The investigation of novel multimetal oxides is a reliable approach for achieving high-performance SIFCs, since the synergetic contributions of various metal ions can effectively enhance the specific capacity and output voltage of materials. In addition, the Li-containing layered oxides synthesized by electrochemical Li–Na ion exchange and Li substitution of transition metals are the valid methods to realize high energy SIFCs.

3.2. Polyanionic Compounds-Based SIFCs

Among various electrodes, polyanionic compounds have attracted immense attention in both the academic world and industrial community since the discovery of the electrochemically active $LiFePO_4$.[81,82] Though, the materials inherently suffer from relatively low theoretical gravimetric capacity resulting from the existence of "heavy" polyanion groups, they offer an extremely stable open framework with structural diversity, as well as strong inductive effect of the anions. They are usually characterized by a long cycle-life, enhanced rate capability, and high safety cathode.[11]

3.2.1. Phosphates

As the counterpart of $LiFePO_4$, olivine $NaFePO_4$ has gained huge attention as it offers a high theoretical capacity of 154 mAh g^{-1} and an operating potential of 2.9 V.[83] However, olivine $NaFePO_4$ is not the thermodynamically stable phase and cannot be synthesized through traditional solid-state methods, while the thermodynamically stable maricite structure usually is regarded as an electrochemically inactive phase owing to the lack of a cationic transport channel.[84,85] Recently, a flexible, solid-state SIFC consisted of an olivine $NaFePO_4$ cathode, hard-carbon anode, and NASICON ($Na_3Zr_2Si_2PO_{12}$)-based composite hybrid solid electrolyte is reported.[86] The hybrid solid electrolyte shows a wide electrochemical window, high ionic conductivity, and high thermal stability, which is beneficial for the full-cell performance-optimization. This pouch-type, flexible full cell exhibits an average voltage of 2.6 V, and yields a discharge capacity of 120 mAh g^{-1} at 0.2 C, with good capacity retention of 96% after 200 cycles. The performance of the full cell at 0.2 C-rate after cycling at 1 C is almost identical to its initial behavior, suggesting that the interfacial characteristics between the electrodes and hybrid solid electrolyte maintain stable during cycling.

As a typical NASICON structure material, $Na_3V_2(PO_4)_3$ (NVP) is widely deemed to be a promising candidate for SIFCs, owing to the stable open-frameworks structure and high operating voltage of 3.4 V.[87–90] Jian et al.[91] reported the detailed structure of rhombohedral $Na_3V_2(PO_4)_3$ and its sodium extracted phase of $NaV_2(PO_4)_3$. It is confirmed that there are two different types of Na sites (6b, M1 and 18e, M2) with different coordination environments in

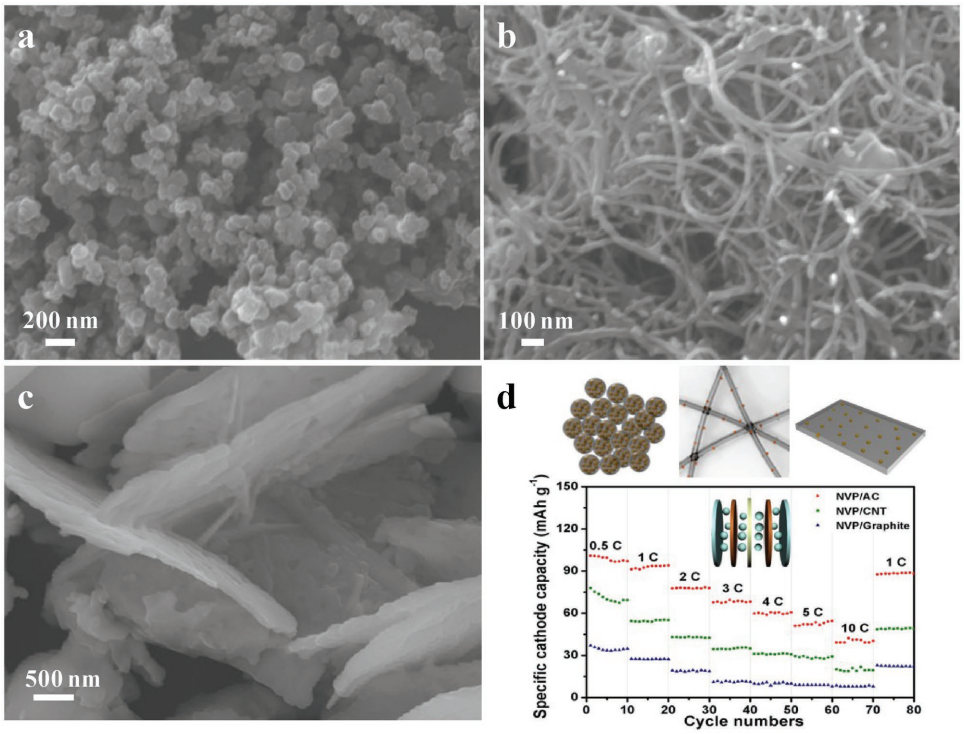

Figure 6. SEM images of a) $Na_3V_2(PO_4)_3$/AC, b) $Na_3V_2(PO_4)_3$/CNT, and c) $Na_3V_2(PO_4)_3$/graphite, respectively. d) Rate performance of $Na_3V_2(PO_4)_3$/AC, $Na_3V_2(PO_4)_3$/CNT and $Na_3V_2(PO_4)_3$/graphite in symmetric sodium-ion batteries. Reproduced with permission.[92] Copyright 2014, Wiley–VCH.

$Na_3V_2(PO_4)_3$. When Na ions deinsert from $Na_3V_2(PO_4)_3$ to form $NaV_2(PO_4)_3$, only Na ions located at the M2 site are extracted and the rest of Na ions still remain at M1 site. Considering the high ionic conductivity, the poor electronic conductivity of these types of materials limits the chemical diffusion; the construction of efficient electronically conducting networks is of great importance. So far, nanominiaturization and surface decoration are the most valid approaches to realize high-rate and long cycle-life $Na_3V_2(PO_4)_3$-based electrodes. Mai's group[92] reported the synthesis of $Na_3V_2(PO_4)_3$ nanograins dispersed in different carbon matrices via a facile method (**Figure 6**a–c). The $Na_3V_2(PO_4)_3$ electrode materials regarding various carbon decoration method are compared, and the mechanism of sodium diffusion pathways in different carbon matrix dimensions is investigated for the first time. $Na_3V_2(PO_4)_3$ nanograins dispersed in acetylene carbon exhibits the best electrochemical properties, thus making it a promising candidate for SIFCs. $Na_3V_2(PO_4)_3$/AC cathode shows a discharge capacity of 117.5 mAh g^{-1} at 0.5 C, approximately 100% of the theoretical capacity of $Na_3V_2(PO_4)_3$, and a very stable cycling performance of 96.4% capacity retention at a 5 C rate over 200 cycles. A symmetric $Na_3V_2(PO_4)_3$ SIFC is also presented, and it exhibits superior cycling performance of 80% capacity retention after 200 cycles at 1 C, and can tolerate a very high current density of 10 C (Figure 6d). However, the average voltage for $Na_3V_2(PO_4)_3$-based symmetric SIFCs is quite low at about 1.7 V,[93,94] other prototype asymmetric SIFCs should be developed.[95] Ren et al.[96] recently reported the controllable synthesis of three-dimensional $Na_3V_2(PO_4)_3$ nanofiber network via a facile self-sacrificed template method (**Figure 7**a). The outside-in morphological evolution mechanisms from microsphere to 3D nanofiber network are systematically investigated based on time-dependent experiments. The $Na_3V_2(PO_4)_3$ cathode material exhibits distinguished cycling stability of 95.9% capacity retention over 1000 cycles at 10 C, and excellent high-rate performance (94 mAh g^{-1} at 100 C) for sodium-ion half-cell, which is attributed to its multi-channel diffusion pathway, continuous electronic conduction, and improved structural integrity. Notably, a novel $Na_3V_2(PO_4)_3$//$NaTi_2(PO_4)_3$ full cell based on NASICON conduction is fabricated (Figure 7b). It displays outstanding cycling stability (96.9% capacity retention over 300 cycles at 5 C) and superior rate capability (80 mAh g^{-1} at 50 C) (Figure 7c), as well as high power density (6 kW kg^{-1}), demonstrating a great potential for high-power application. To improve the energy density of $Na_3V_2(PO_4)_3$-based full cells, a hard-carbon anode with high specific capacity and low average voltage has also been applied. It, however, fails to realize high energy density due to large polarization.[91,97] In order to solve this problem, Mai's group[98] proposed a polarization suppresssion strategy to improve the output voltage of the full cell. The NVP//hard-carbon (HC) full cell with a 3.3 V high voltage has been fabricated based on the easily scalable synthesized 3D interconnected NVP cathode (NVP-NP) and biomass-method-fabricated HC anode. Through promoting the electronic conductivity and ionic diffusion rate of NVP-NP, the NVP-NP//HC full cell shows substantial increases in the energy density (≈20%) compared with the bulk/bare samples (Figure 7d–f).

Recently, vanadyl phosphate ($VOPO_4$) materials have emerged as an alternative cathode for SIFCs, owing to its

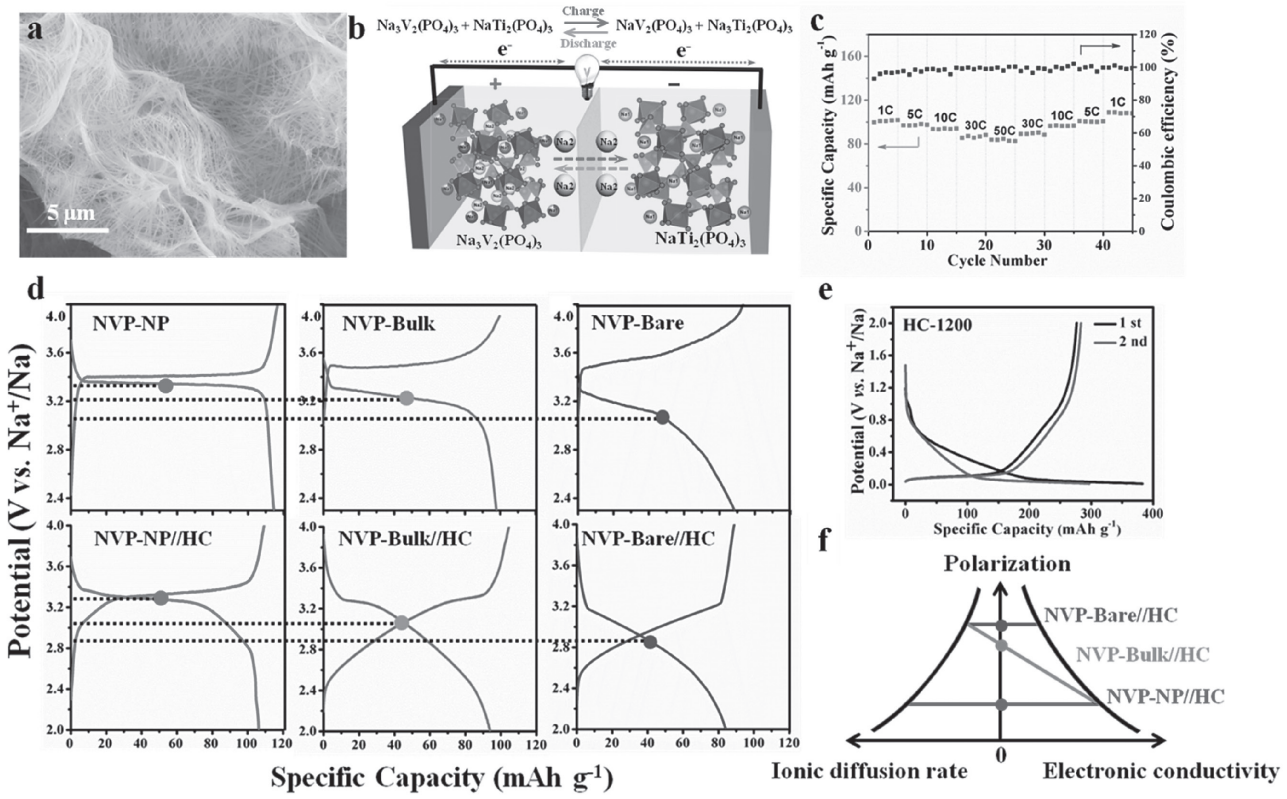

Figure 7. a) SEM image of NVP nanowire network. b) Schematic illustration of the NVP//NTP full cell. c) Rate capability of the NVP-F-based full cell. Reproduced with permission.[96] Copyright 2016, Elsevier. d) The second charge/discharge curves of NVP-NP and NVP-NP//HC (left), NVP-Bulk and NVP-Bulk//HC (middle), NVP-Bare and NVP-Bare//HC (right) at 0.2 C. e) The charge/discharge curves of HC-1200 at 60 mA g^{-1}. f) Schematic illustrations of the relationship among polarization, ionic diffusion rate, and electronic conductivity. Reproduced with permission.[98] Copyright 2016, Elsevier.

high operating voltage, good structure stability, and relatively high specific capacity.[99] A new $VOPO_4$//$Na_2Ti_3O_7$ SIFC has been developed by Yu's group.[100] **Figure 8**a displays the CV and charge–discharge curves of $VOPO_4$ (2.5–4.3 V) with an oxidation peak at 3.75 V and a reduction peak at 3.4 V, which is attributed to the redox reaction of V^{5+}/V^{4+}. Accordingly, $Na_2Ti_3O_7$ exhibits a distinct redox peak at about 0.55 V, corresponding to Ti^{4+}/Ti^{3+} reaction. The full cell is able to deliver a high specific capacity of 114 mAh g^{-1} at 0.1 C as well as an exceptionally high energy density of 220 Wh kg^{-1}. It is, however, necessary to reduce the polarization and irreversibility reaction of the electrode materials in the first cycle through pre-sodiation/desodiation processes, which hold back its further application. Other phosphate-based SIFCs such as $Na_3V_2(PO_4)_3$//$ATiOPO_4$ have also been studied.[101]

3.2.2. Fluorophosphates

$Na_3V_2(PO_4)_2F_3$ (NVPF) has attracted considerable attention in view of its high theoretical capacity (128 mAh g^{-1} for the oxidation of V^{3+}/V^{4+}) and high voltage plateaus at 3.68 and 4.15 V vs Na^+/Na, which endows it a great potential for a high energy SIFC cathode.[102] A $Na_3V_2(PO_4)_2F_3$// hard-carbon full cell operating in various electrolyte has been explored.[103] It is found that the optimum composition of electrolyte is $EC_{0.45}$:$PC_{0.45}$:$DMC_{0.1}$, which provides low resistivity of the SEI, resulting in good rate capability and high capacity during cycling. The $Na_3V_2(PO_4)_2F_3$//hard-carbon full cell displays an operation voltage of 3.65 V with very low polarization, as well as excellent capacity retention with 97 mAh g^{-1} after more than 120 cycles. In addition, the preparation of Na-enriched phases is of great significance for highly-efficient Na-ion batteries, since the extra Na ions present in NVPF can be removed at low potential without an added weight penalty. An Na-enriched '$Na_{3+x}V_2(PO_4)_2F_3$' cathode has been synthesized through a simple ball milling approach, and the three distinct Na sites are all seven-fold coordinated with four oxygen and three fluorine atoms, which is analogous to the coordination of Na1 in NVPF (Figure 8b). The structural analysis fully confirms the chemical composition ($Na_4V_2(PO_4)_2F_3$) and indicates that there is apparently no further space for Na insertion. The corresponding '$Na_{3.5}V_2(PO_4)_2F_3$'//hard-carbon full cell exhibits both enhanced specific capacity and cycling stability compared to the conventional one (Figure 8c).[19] Tarascon's group[38] reported a simulation approach to estimate the energy density of SIFCs through measuring the effect of various parameters, such as the ratio of positive to negative electrodes ($R_{P/N}$), the charge and discharge cut-off voltages, and the addition of an Na source to the positive electrode. The $Na_3V_2(PO_4)_2F_3$//C full cells were predicted to have an optimum energy density of 243 Wh kg^{-1} (based on the weight of cathode and anode) in an $R_{P/N}$ of 2.65 when cycled between 2 and 4.3 V, and the feasibility to obtain 267 Wh kg^{-1} by using $Na_{3.45}V_2(PO_4)_2F_3$

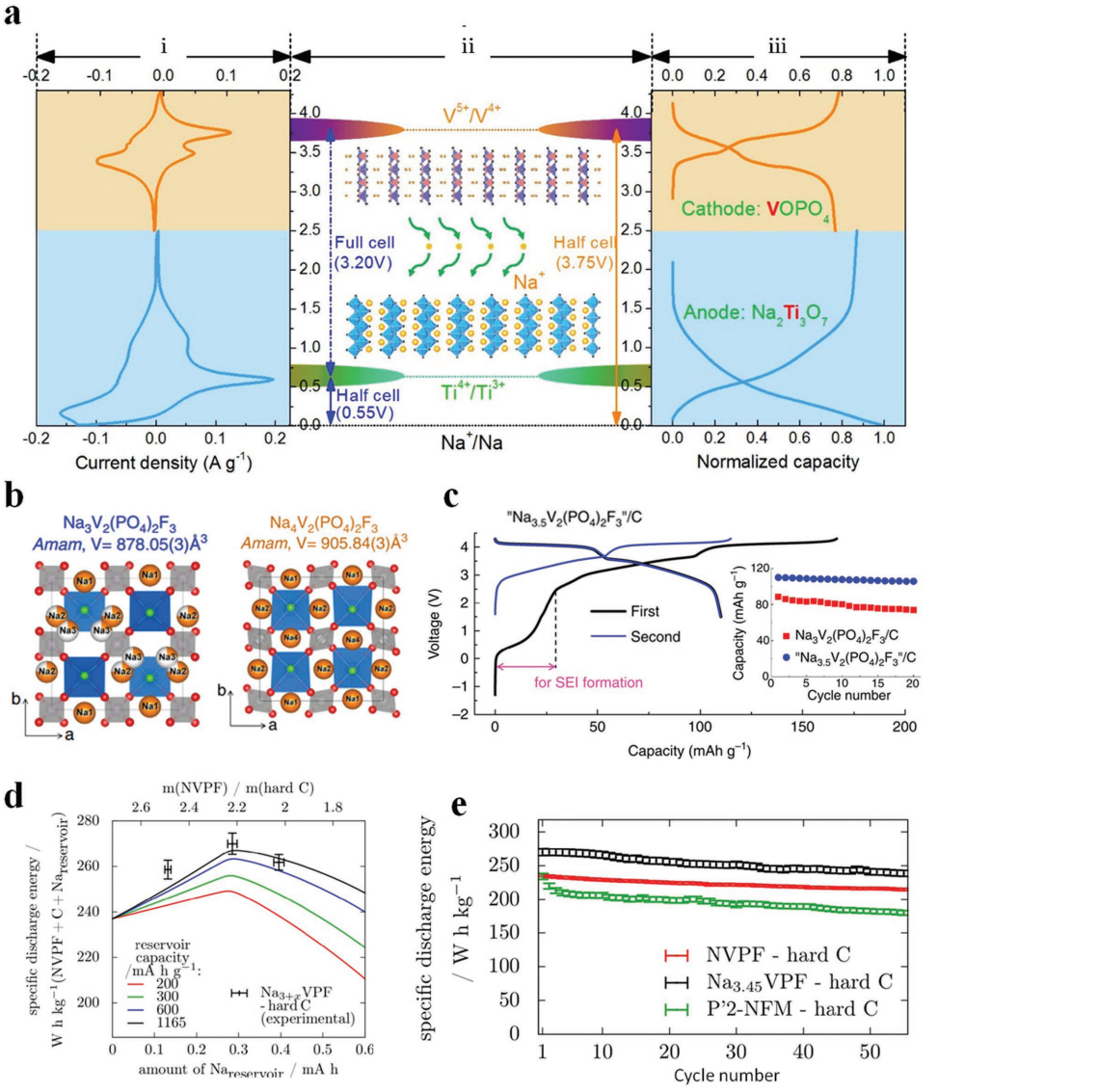

Figure 8. a) Electrochemical characteristics of $Na_2Ti_3O_7$ and $VOPO_4$ electrodes in the half-cell format vs Na^+/Na. Reproduced with permission.[100] Copyright 2016, Royal Society of Chemistry. b) Structure of $Na_3V_2(PO_4)_2F_3$ and $Na_4V_2(PO_4)_2F_3$. c) The charge–discharge profiles of '$Na_{3.5}V_2(PO_4)_2F_3$' in the full cell. Reproduced with permission.[19] Copyright 2016, Nature Publishing Group. d) Specific energy of simulated full cells (lines) as a function of the capacity provided by the sodium reservoir additive for different values of the specific capacity of the additive. e) Discharge energy measured during galvanostating cycling of Na_3VPF/hard C, $Na_{3.45}VPF$/hard C and P′2-NFM/hard C cells with 4.3 V higher cutoff voltage. Reproduced with permission.[38] Copyright 2016, The Electrochemical Society.

phase as a host material (Figure 8d,e). Other prototype $Na_3V_2(PO_4)_2F_3$//$NaTi_2(PO_4)_3$,[104] $NaVPO_4F$//hard-carbon[105] SIFCs have also been reported.

3.2.3. Pyrophosphates

Pyrophosphate compounds offer a robust three-dimensional $(P_2O_7)^{4-}$-framework, multidimensional ionic conduction pathways, and rich structural variation.[106] However, there are only a few scientific papers focusing on the pyrophosphate-based SIFCs. As a high voltage pyrophosphate cathode, $Na_4Co_3(PO_4)_2P_2O_7$ possesses the multi redox couples in the potential region of 4.1 and 4.7 V, and is able to offer the discharge capacity of 95 mAh g^{-1}, corresponding to 2.2 Na^+ insertion/extraction in $Na_4Co_3(PO_4)_2P_2O_7$.[107] The $Na_4Co_3(PO_4)_2P_2O_7$//hard-carbon is found to deliver an ultrahigh operating voltage of about 4.1 V and exhibits the capacity retention of 83% after 100 cycles. As another new type pyrophosphate material, $Na_{3.12}Fe_{2.44}(P_2O_7)_2$ owns a theoretical capacity of 117.4 mAh g^{-1}, and has been studied as the cathode of $Na_{3.12}Fe_{2.44}(P_2O_7)_2$/MWCNT//carbon-black full cell.[108] The full cell delivers a capacity of 145 mAh g^{-1} at 100 mA g^{-1} (based on carbon black negative mass) and a Coulombic efficiency of 70%, with an average operation voltage of around 2.8 V. The capacity of the full cell fades to 81 mAh g^{-1} after 50 cycles, indicating a poor cycling performance due to the inappropriate ratio of positive to negative electrodes.

In short, although polyanionic compounds suffer intrinsically from a relatively low theoretical gravimetric

capacity due to the presence of $(XO_4)^{n-}$ groups, they still have been adopted as the star cathode materials for SIFCs due to their excellent structural stability and diversity, as well as the high output voltage. The main strategy for promoting the electrochemical performance of polyanionic-based SIFCs is to enhance their low electronic conductivity, such as morphological modification and carbon decoration. Notably, the NASICON $Na_3V_2(PO_4)_3$ and fluorophosphate $Na_{3+x}V_2(PO_4)_2F_3$ are being widely recognized as promising candidates for high-power and high-energy SIFCs due to the ultrafast and ultrastable Na-insertion/deinsertion performance. Thus, the investigations of $Na_3V_2(PO_4)_3$-based SIFCs with promoted energy density and $Na_{3+x}V_2(PO_4)_2F_3$-based SIFCs with enhanced cycling performance are of great importance for the development of high-performance SIFCs.

3.3. Metal-Hexacyanometalates-Based SIFCs

Metal hexacyanometalates $A_xM_1[M_2(CN)_6]_y{\cdot}zH_2O$ (A = alkaline metal; and M_1 and M_2 = transition metal ions;) have an open-framework structure which is fundamentally different from other insertion electrode materials because of its large channels and interstices.[109,110] The framework is consisted of a face-centerd cubic structure of transition metal cations where each cation is octahedrally coordinated to hexacyanometallate groups. It has been considered as a promising class for SIFCs cathode due to high specific capacity, ease of synthesis, and reversible insertion/extraction of Na^+ in a rapid channel.

Goodenough and co-workers[111] reported an effect of interstitial H_2O on the structure and electrochemical properties of sodium manganese(II) hexacyanoferrates(II) with the nominal composition $Na_2MnFe(CN)_6{\cdot}zH_2O$. The removal of interstitial H_2O from the $Na_2MnFe(CN)_6{\cdot}zH_2O$ framework results in a structural transition and a far-reaching electrochemical property change (**Figure 9**a). The newly found dehydrated phase exhibits superior electrochemical performance in half-cell, which delivers a reversible capacity of 150 mAh g^{-1} at 3.5 V (Figure 9b). The SIFCs coupling with hard-carbon anode have also been explored to deliver a reversible capacity of 140 mAh g^{-1} at the voltage range of 1.5 to 3.8 V. It gives a moderate rate performance with 96 mAh g^{-1} at 2 C, and no obvious capacity fade is observed over 30 cycles at 0.7 C. Another novel air-stable sodium–iron hexacyanoferrate (R-$Na_{1.92}Fe[Fe(CN)_6]$) with rhombohedral structure is demonstrated to be a scalable, low-cost cathode material for SIFCs.[112] The ionic insertion/extraction mechanism of the iron redox is investigated and clarified via synchrotron-based soft X-ray absorption spectroscopy, which also reveals the relationship between the physical properties and the electrochemical behaviors of this material. When used as sodium half-cell cathode, it exhibits two discharge plateaus at 3.00 and 3.29 V, with a specific capacity of ≈160 mAh g^{-1} (Figure 9c), as well as excellent reversibility with 80% of the initial capacity retained after 750 cycles. Most importantly, the $Na_{1.92}Fe[Fe(CN)_6]$//hard-carbon full cell is directly assembled without pre-sodiation, owing to the rich sodium content in $Na_{1.92}Fe[Fe(CN)_6]$. The full cell shows an initial charge capacity of 153.1 mAh g^{-1} and a discharge capacity of 119.4 mAh g^{-1}, corresponding to a Coulombic efficiency of 78%, and demonstrates a superior rate capability (Figure 9d). Other metal hexacyanometalates have also been studied as SIFCs cathode, such as $Na_4Fe(CN)_6$/C,[113] $Na_{1.76}Ni_{0.12}Mn_{0.88}$-$[Fe(CN)_6]_{0.98}$,[114] etc.

In brief, the open-framework metal-hexacyanometalates provide fast diffusion of Na ions, in addition to various Na contents and redox couples, which enables it a promising cathode material for SIFCs. Recently, advanced hexacyanometalate-based SIFCs are able to provide reversible capacities of about 120 mAh g^{-1} with average potentials of 3.0 V. Nevertheless, the metal-hexacyanometalates-based SIFCs are always restricted by a low Coulombic efficiency due to the decomposition of the crystal water. The thermal stability of sodiated/desodiated hexacyanometalates needs to be investigated to diagnose the safety concerns of SIFCs. Therefore, full cell fabrication based on crystal-water-free metal-hexacyanometalates materials with less defects is a significant trend in future development.

3.4. Organic-Based SIFCs

Since the development of green and sustainable electrode materials is necessary for safer and low-cost prototype SIFCs, one of the innovative strategies is focusing on novel organic alternatives instead of traditional inorganic compounds, which are able to avoid structural deterioration and rapid capacity fading.[115] Organic-based materials are considered to provide several potential advantages, such as structural diversity and flexibility, molecular level controllability, eco-efficient processability and recyclability.[116] Although various organosulfur compounds, carbonyl compounds, radical compounds, and functional polymers have been studied as the high capacity, long cycle-life, and high rate-capability electrode materials of energy-storage devices, the investigation of SIFCs based on organic electrode materials still needs further explorations.

All organic-based materials are in favor of low-cost SIFC applications. Suga et al.[117] firstly reported an n-type radical-polymer anode coupling with a p-type radical-polymer cathode, and fabricated an all-radical polymer-based battery. Although their group is able to offer bipolar redox to be used as both cathode and anode for constructing a symmetric all-organic battery, these radical batteries have very low working voltage (<1 V) with limited specific capacity (about 50 mAh g^{-1}). Chen's group[118] constructed an all-organic SIFC based on organic tetrasodium salt $Na_4C_8H_2O_6$ by a green and facile method. This novel material can be reversibly used as both a cathode and anode since the two Na^+ in $Na_4C_8H_2O_6$ are separately related to the enolate groups at 1.6–2.8 V and carboxylate groups at 0.1–1.8 V, delivering specific discharge capacities of about 180 mAh g^{-1} with Coulombic efficiency reaching up to 100%. Notably, the symmetric all-organic-based SIFC is found to provide an average output voltage of 1.8 V, with an energy density of about 65 Wh kg^{-1} (total mass), as well as a moderate capacity retention of 76% after 100 cycles. More recently, Chen and

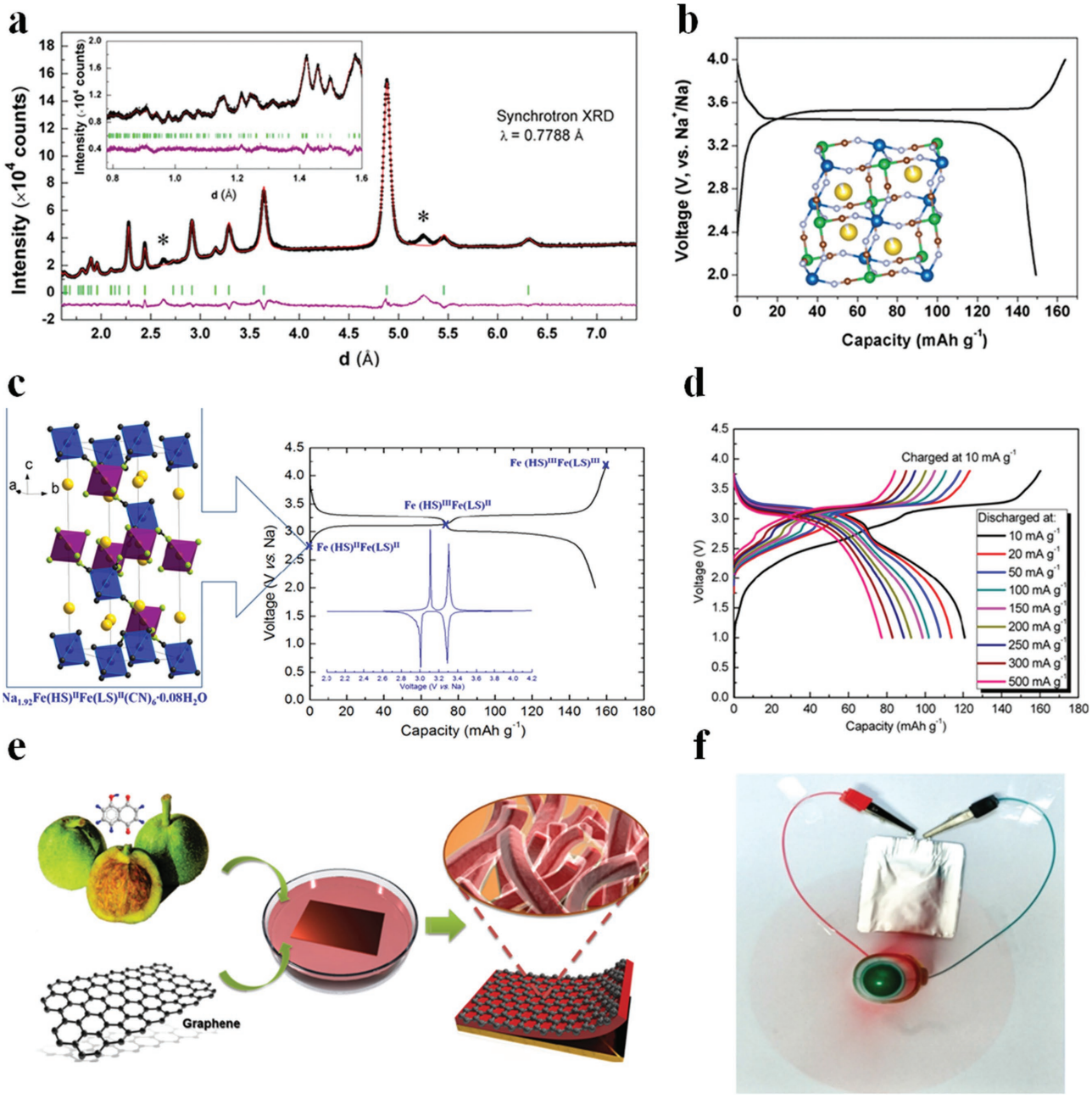

Figure 9. a) Synchroton X-ray diffraction (SXRD) patterns of R-$Na_{2-\delta}$MnHCF. b) Galvanostatic initial charge and discharge profiles of vacuum-dried R-$Na_{2-\delta}$MnHCF at a current of 0.1 C (15 mA g^{-1}). Reproduced with permission.[111] Copyright 2015, American Chemical Society. c) Galvanostatic charge and discharge curves at a current of 10 mA g^{-1} at the first cycle (chronoamperograms were embedded) along with crystal structure. d) Discharge curves of the R-FeHCF//hard-carbon full cell at different currents. Reproduced with permission.[112] Copyright 2015, American Chemical Society. e) Fabrication process of Juglone/RGO electrodes. f) An aluminum-pouch-type full battery used to power an electric fan. Reproduced with permission.[119] Copyright 2015, Wiley–VCH.

co-workers[119] presented a biomolecule-Juglone-based electrode through a facile and scalable self-assembly process, free from any binder or additional conductive (Figure 9e). The pouch-type SIFCs are assembled (Figure 9f) based on the biomass Juglone/RGO anode, $Na_3V_2(PO_4)_3$/C cathode, and copper grids as the substrate. This SIFC exhibits an operating voltage of about 1.4 V, with a cycling stability of 91.8% after 100 cycles. Other organics, such as $Na_2C_6O_6$,[120] polyimide,[121] and all-organic polymeric-based[122,123] SIFCs have also been investigated.

In short, the advantages of sustainability, cheapness, and high specific capacity make organic materials become attractive candidates for green SIFCs. While, the intrinsic low electronic conductivity and easily dissolution of the material are the main challenges that should be paid particular attention. Despite various strategies, such as carbon decoration, encapsulation, and electrolyte solidification, that have been conducted to improve their electrochemical performances, the SIFCs based on organic materials still need more systematic study to achieve high operating voltage and long cycle-life.

Table 1. Electrochemical behaviors of cathode-based SIFCs.

Cathode	Anode	Voltage (V)	Capacity (mA h g^{-1})	Energy Density (Wh kg^{-1})
$Na_{0.44}MnO_2$[48]	pyrolyzed carbon	2.7	106 (0.5 C)	160–200
$Na_{0.7}MnO_{2.05}$[211]	carbon nanofibers	1.8	106 (100 mA g^{-1})	90–110
$NaCrO_2$[54]	Sb–C	2.2	92 (0.1 C)	160–180
$NaCrO_2$[52]	hard carbon	3.0	102	210–230
$Na_{0.7}CoO_2$[44]	graphite	2.2	80 (1 C)	80–100
$NaNi_{0.5}Mn_{0.5}O_2$[63]	Sn–C	2.5	125 (0.2 C)	230–250
$NaNi_{0.5}Mn_{0.5}O_2$[62]	hard carbon	/	115 (0.1 C)	210–230
$Na_3Ni_2SbO_6$[61]	Sb–C	2.4	105 (0.1 C)	190–210
$Na_{0.8}Ni_{0.4}Ti_{0.6}O_2$[60]	$Na_{0.8}Ni_{0.4}Ti_{0.6}O_2$	2.7	82 (0.2 C)	120–140
$Na_{0.78}Li_{0.18}Ni_{0.25}Mn_{0.583}Ow$[77]	SnS_2	2.5	210 (0.07 C)	310–350
$Na[Ni_{1/3}Fe_{1/3}Mn_{1/3}]O_2$[69]	hard carbon	3.0	120 (0.2 C)	240–260
$Na[Ni_{0.25}Fe_{0.5}Mn_{0.25}]O_2$[70]	Fe_3O_4	2.4	130 (0.1 C)	190–210
$Na_{0.66}Ni_{0.17}Co_{0.17}Ti_{0.66}O_2$[66]	$Na_{0.66}Ni_{0.17}Co_{0.17}Ti_{0.66}O_2$	3.1	–	90–100
$Na[Ni_{0.6}Co_{0.05}Mn_{0.35}]O_2$[18]	hard carbon	2.7	141 (1 C)	240–260
$Na_{0.6}Ni_{0.22}Fe_{0.11}Mn_{0.66}O_2$[212]	Sb–C	2.7	120 (0.07 C)	230–250
$Na_{0.6}Ni_{0.22}Fe_{0.11}Mn_{0.66}O_2$[213]	Sb–C	2.7	120 (0.05 C)	230–250
$Na_{0.9}[Cu_{0.22}Fe_{0.30}Mn_{0.48}]O_2$[67]	hard carbon	3.2	86 (0.5 C)	200–220
$Na_{0.61}[Mn_{0.27}Fe_{0.34}Ti_{0.39}]O_2$[214]	hard carbon	3.3	–	210–230
$Na[Li_{0.05}(Ni_{0.25}Fe_{0.25}Mn_{0.5})_{0.95}]O_2$[80]	hard carbon	3.4	177 (0.1 C)	360–380
$NaFePO_4$[215]	Sn–C	2.7	140 (0.1 C)	280–300
$NaFePO_4$[86]	hard carbon	2.3	120 (0.2 C)	190–210
$Na_3V_2(PO_4)_3$[94]	$Na_3V_2(PO_4)_3$	1.7	105 (0.25 C)	50–70
$Na_3V_2(PO_4)_3$[132]	graphite	2.7	109 (0.2 C)	160–180
$Na_3V_2(PO_4)_3$[97]	hard carbon	1.6	116 (5 C)	130–150
$Na_3V_2(PO_4)_3$[96]	$NaTi_2(PO_4)_3$	1.3	100 (5 C)	60–80
$Na_2Fe_2(SO_4)_3$[140]	carbon nanofiber	3.5	70 (–)	180–200
$Na_3V_2(PO_4)_2F_3$[104]	$NaTi_2(PO_4)_3$	1.6	108 (0.2 C)	80–100
$Na_3V_2(PO_4)_2F_3$[103]	hard carbon	3.7	105 (0.2 C)	270–290
$Na_{3.45}V_2(PO_4)_2F_3$[38]	hard carbon	3.7	109 (0.1 C)	280–300
$Na_{3.5}V_2(PO_4)_2F_3$[19]	hard carbon	3.7	110 (0.2 C)	280–300
$Na_4Co_3(PO_4)_2P_2O_7$[107]	hard carbon	4.1	92	280–300
$Na_{3.12}Fe_{2.44}(P_2O_7)_2$[108]	carbon black	2.5	–	140–160
$Na_{1.76}Ni_{0.12}Mn_{0.88}[Fe(CN)_6]_{0.98}$[114]	hard carbon	3.0	91 (1 C)	200–220
$Na_2MnFe(CN)_6{\cdot}zH_2O$[111]	hard carbon	3.2	105 (0.7 C)	230–250
$Na_{1.92}Fe[Fe(CN)_6]$[112]	hard carbon	3.0	120 (0.07 C)	240–260
$Na_xFeFe(CN)_6$[166]	FeOx	1.7	100 (0.2 C)	120–140
poly(galvinoxylstyrene)[117]	poly(galvinoxylstyrene)	0.7	27 (5 C)	10–30
$Na_2C_6O_6$[120]	hard carbon	2.1	179 (0.1 C)	220-240
polytriphenylamine[123]	poly(anthraquinonyl sulphide)	1.5	–	80–100

3.5. Comparisons of Cathode-Based SIFCs

In order to systematically compare and analyze the electrochemical properties of the main cathode-materials-based SIFCs, we summarize their average operating voltages, specific discharge capacities and energy density. The detailed definitions of different parameters in **Table 1** are as follows: 1) "Voltage" represents the average operating voltage of the full cell; 2) the calculation of "Capacity" is based on the mass of cathode active material in the full cell; 3) "Energy density" represents the estimated specific gravimetric energy of the full cell under the optimized electrode matching condition, and the calculation of "Energy density" is based on the total mass of active materials. Besides, the calculation methods for "Capacity", "Energy Density", and "Voltage" in the references are multifarious, such as based on the mass of

cathode, anode, or total active materials. In order to ensure that our comparisons are under the consistent standard, partial "Capacity" and "Energy Density" have been recalculated.[36,37] Although we sincerely respect the data in the references, some slight inevitable discrepancies may exist in the recalculation processes.

The metal-oxides-based SIFCs exhibit outstanding discharge capacities, some even reaching 210 mAh g^{-1}, and the energy density of a certain type of SIFCs is as high as ≈380 Wh kg^{-1}. However, the high capacity always suffers from deep insertion/deinsertion of Na ions, which inevitably induces large expansion and shrinkage of the lattice volume and easily causes irreversible structural degradation, resulting in severe capacity decline during extended cycling. To balance the energy density and cycling stability of the full cell, exploring suitable multimetal oxides based on rational synergetic effect of various metal ions with enhanced operating voltage and relatively high structural stability is a resultful strategy. Polyanionic-compounds-based SIFCs possess high operating potential (≈4.1 V) and ultralong cycle-life (restricted by anode material) due to the stable framework structure and the inductive effect of the anions. However, the relatively low discharge capacity (around 120 mAh g^{-1}) and the heavy $(XO_4)^{n-}$ group seriously limit the specific gravimetric energy of the full cells. Investigating novel Na-rich polyanionic-based SIFCs is a promising direction in terms of high specific capacity. The metal-hexacyanometalates-based SIFCs are able to deliver an average operating voltage of 3.0 V with specific capacity of 110 mAh g^{-1}. Besides, the low Coulombic efficiency owing to the decomposition of the crystal water and the undesirable thermal stability of the full cell should be further improved before application. Scientific researches focusing on the metal-hexacyanometalates-based SIFCs remain insufficient and need more exploration. The advantages of low cost and high specific capacity (≈200 mAh g^{-1}) enable the organic materials as promising materials for SIFCs. Nevertheless, the low energy density of organic-based SIFCs is attributed to the lack of investigations in proper electrode couples. The undesirable electronic conductivity and high material dissolution, which gravely limit its development, should be tackled through material encapsulation, electrolyte optimization, and carbon decoration before wide spread applications. Based on the overall electrochemical behaviors, phosphates and metal oxides are currently the most promising cathode candidates for SIFCs benefited from the high energy density and good cycling stability.

4. Non-Aqueous Anode-based SIFCs

Compared with lithium, sodium metal has a higher chemical activity with poor processability, and cannot be directly used as an anode, considering its safety hazard and unstable passivation layer in most organic solvents at room temperature. Sodium anode materials have to bear more unpredictable electrochemical behaviors and structural evolution during insertion/deinsertion due to the large ionic radius of the Na ion.[17] Besides, the relatively-low initial Coulombic efficiency of the sodium anode materials further hinders in the assembly of full cells. It is therefore urgently needed to explore suitable anode materials with an appropriate operating voltage, high reversible capacity, and acceptable initial Coulombic efficiency. So far, various anode materials have been investigated and can be classified into carbonaceous materials, sodium alloy, metal oxides/sulfides, phosphorus, etc.

4.1. Carbonaceous-Based SIFCs

The most widely studied anode for SIBs are carbonaceous materials; this is attributed to their natural abundance, low cost, and environmental friendly.[124–127] Graphite, which is commonly used as a high-performance anode for commercial LIBs, is electrochemically less active in SIBs, owing to its relatively small interlayer distance (d_{002} = 0.334 nm) for Na-ion intercalation.[17] To overcome these limitations, Wen et al.[128] proposed chemically modified graphite as an anode for SIBs with an enlarged interlayer lattice distance. The expanded graphite is a graphite-derived material formed by a two-step oxidation–reduction process that retains the long-range-ordered layered structure of graphite, yielding a generally large interlayer distance (>0.34 nm; **Figure 10**a–c). These features provide favorable conditions for electrochemical intercalation of Na ions. Moreover, Jache et al.[129] reported a new strategy to apply graphite as the anode for SIBs, where Na storage in graphite occurs via co-intercalation with diglyme electrolyte. More recently, Kang's group[130] revealed an unusual Na-storage behavior in natural graphite, where Na^+-solvent co-intercalation occurs, combined with partial pseudocapacitive behaviors, when utilizing ether-based electrolytes. A $Na_{1.5}VPO_{4.8}F_{0.7}$//graphite full cell with the $NaPF_6$ in diethylene glycol dimethylether (DEGDME) electrolyte is also constructed and exhibits an average discharge voltage of 2.9 V. The specific energy of the system is about 120 Wh kg^{-1} (based on the total mass of active materials) and still maintains 70% of the initial capacity after 250 cycles. Flexible polyimide graphite films have a highly in-plane ordered structure, which results in the enhanced electrical conductivity and excellent mechanical strength.[131] A novel porous graphite film for an integrated anode through laser drilling technique has been reported.[132] It displays moderate discharge capacity of 127 mAh g^{-1} with superior cycling stability for 1000 cycles. The practicability of graphite film in an Na full cell is also confirmed in conjunction with the $Na_3V_2(PO_4)_3$ cathode in 1 M $NaPF_6$/diglyme electrolyte. It exhibits the energy of 130.7 Wh kg^{-1} based on the total electrode materials with excellent cycling stability (92% after 500 cycles). The rate capability of the full cell is also studied and even at a high current density of 500 mA g^{-1}, the capacity retention is still as high as 76.7% in comparison with the initial state. Chen's group[133] reported the high-rate graphite as an anode material for SIFCs by coupling with an $Na_3V_2(PO_4)_3$ cathode in some linear ether-based electrolytes. The reversible capacity of the full cell is retained at ≈80 mAh g^{-1} even at a high current density of 2 A g^{-1}, demonstrating a superior high rate capability. It also exhibits outstanding cycling performance, with capacity retention of ≈80% after 400 cycles. Although the cycling stability and rate capability of the

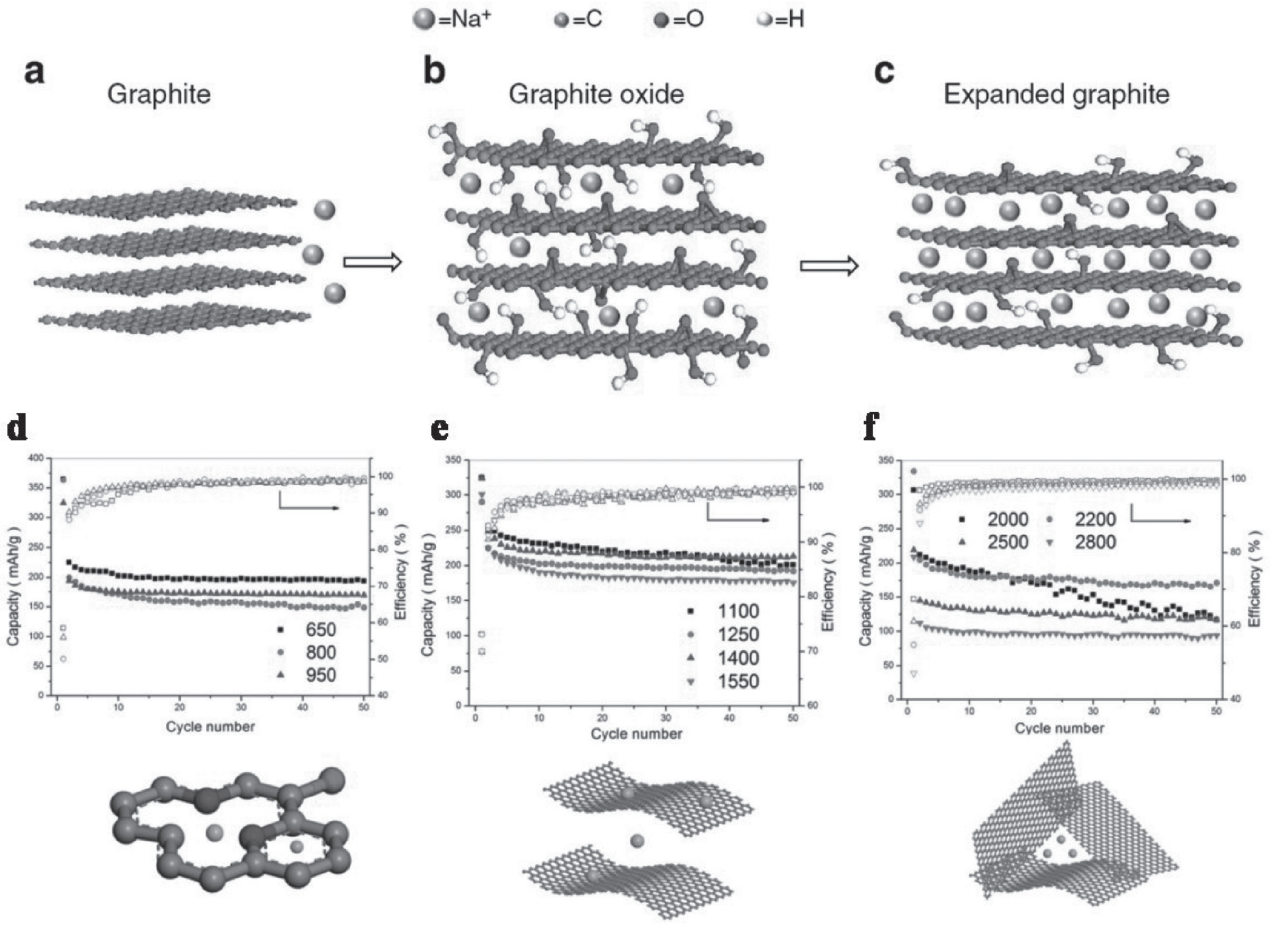

Figure 10. a) Na^+ cannot be electrochemically intercalated into graphite because of the small interlayer spacing. b) Electrochemical intercalation of Na^+ into GO is enabled by the enlarged interlayer distance because of oxidation. However, the intercalation is limited by steric hindering from large amounts of oxygen-containing groups. c) A significant amount of Na^+ can be electrochemically intercalated into EG owing to suitable interlayer distance and reduced oxygen-containing groups in the interlayers. Reproduced with permission.[128] Copyright 2014, Nature Publishing Group. d–f) Discharge capacity retention (upside) and schematic representation of Na-ion storage mechanisms (underside) in stage I, stage II, and stage III. Reproduced with permission.[140] Copyright 2015, Wiley–VCH.

graphite have been significantly promoted, its relatively low specific capacity is not encouraging and urgently needs substantial improvement.

To find a high-capacity alternative anode for SIFCs, hard carbon (non-graphitizable amorphous carbon) has been investigated thoroughly due to its highly disordered structure and large interlayer distance.[134] Several hard carbons have demonstrated a high reversible capacity of about 300 mAh g^{-1}, and their overall sodium-storage mechanisms can be attributed to chemisorption on surface heteroatoms,[135] metal nanopore filling,[124] intercalation between graphene layers,[136] and reversible adsorption at structural defect sites in the graphene.[137] Despite its insufficient cycle-life and poor rate capability in early reports, the high reversible capacity of hard carbon is close to the graphite anode in LIBs, which endows it a great potential to be used as promising anode for SIFCs.

Komaba et al.[138] initially reported a high capacity and excellent reversibility SIFC based on a hard-carbon anode and a layered $NaNi_{0.5}Mn_{0.5}O_2$ cathode in propylene carbonate electrolyte solutions. The $NaNi_{0.5}Mn_{0.5}O_2$//hard-carbon full cell exhibits a high reversible capacity more than 200 mAh g^{-1}, and an average output voltage of 2.8 V at the current density of 25 mA g^{-1}. Notably, even tested at a higher rate of 300 mAh g^{-1}, no significant capacity decrease is observed, indicating the remarkable rate capability of the full cell. The thermal adaptability of the anode material is also a significant parameter, especially in full cell applications. The operating condition of hard carbon in a wide range of temperature from -10 to 90 °C has been addressed.[139] It is noted that the electrochemical performance of hard carbon electrodes is strongly affected by the working temperature, and it exhibits a specific discharge capacity of 274 mAh g^{-1} at 90 °C, which decreases rapidly to 175 mAh g^{-1} at 25 °C, and becomes nearly inactive when working under 0 °C. An $NaCrO_2$//hard-carbon full cell shows a high, reversible discharge capacity of 260 mAh g^{-1} at 90 °C with an average voltage of ≈2.8 V. Understanding the microstructure, morphology, and surface functionality of hard carbon is of great importance for promoting the Na-storage abilities and thus achieving high performance. Tarascon and co-workers[140] reported the carbon nanofibers prepared via electrospinning method and its applications in $Na_2Fe_2(SO_4)_3$//carbon-nanofibers full cell. The detailed structures of the carbon nanofibers are tailored

through pyrolyzation at various temperatures ranging from 650 to 2800 °C. The degree of graphitization and heteroatoms of carbon nanofibers have been controlled through different calcination temperatures, enabling to establish a correlation between the carbon-nanofibers characteristics and Na-storage properties (Figure 10d–f). For stage I CNFs (650–950 °C), the voltage profiles show initially a pseudo plateau followed by a monotonous decrease of the voltage to 0 V, with therefore a large irreversibility between the first discharge and charge so that the reversible capacity is limited to about 200 mAh g^{-1}. For CNFs locating to stage II (1100–1550 °C), the voltage profile can be divided into two regions, that is the sloping region between 1 and 0.1 V and a flat plateau region at ≈0.1 V. As for stage III CNFs (above 2000 °C), the materials prepared in this temperature interval present a high degree of graphitization, small mesopores, and low active surface area, resulting in low reactivity with the electrolyte. The initial Coulombic efficiency of the anode has always been an intractable problem, which is deadly important before full cell applications. Li et al.[141] proposed the synthesis of monodispersed hard-carbon spherules from an abundant biomass of sucrose, and the initial Coulombic efficiency was promoted to 83% via coating the soft carbon on its surface through the pyrolysis of toluene. The viability of hard-carbon spherules in an SIFC is also confirmed in conjunction with the P2-$Na_{2/3}Ni_{1/3}Mn_{2/3}O_2$ cathode material. The full cell shows a high initial Coulombic efficiency of 76%, outstanding cycling performance (73% after 150 cycles), and superior operating voltage of 3.5 V. An amorphous carbon material fabricated from low-cost pitch was also investigated.[142] When evaluated as $Na_{0.9}[Cu_{0.22}Fe_{0.30}Mn_{0.48}]O_2$//amorphous-carbon full cell, it exhibits a mean output voltage of 3.2 V and a high initial Coulombic efficiency of 78%, with capacity retention of 97% after 100 cycles. Biomass approach is known as an environmentally friendly and easily scalable method for the synthesis of electrode materials.[143,144] Wu et al.[145] reported an apple-biowaste-derived hard carbon which showed excellent electrochemical performance as a sodium half-cell. The SIFC with P2-$Na_xNi_{0.22}Co_{0.11}Mn_{0.66}O_2$ as the cathode is revealed to have a stable cycling performances (81% after 100 cycles) with specific capacity as high as 250 mAh g^{-1} (based on hard carbon).

In short, hard carbon has been adopted as most promising anode for SIFCs owing to its high reversible capacity, low operating voltage, and low-cost. However, the poor rate capability and limited cycle-life of hard carbon seriously limit its application. Nanofunctionalization, electrolyte optimization, heteroatom doping, and controlled pyrolyzation are considered as the effective methods for improving Na storage properties of hard carbon. In this contribution, the developments of hard-carbon-based SIFCs with enhanced cycle-life, high initial Coulombic efficiency, as well as acceptable rate capability are the major pursuit in the near future.

4.2. Alloy-Based SIFCs

Alloy-based materials have attracted growing attention due to their high theoretical capacity compared with carbon-based materials.[146] Ceder's group[147] reported that a high theoretical capacity of 847 mAh g^{-1} can be achieved from Sn to $Na_{15}Sn_4$. Darwiche et al.[148] revealed that the insertion of Na into Sb was able to form the intermediate phases Na_xSb, which delivered a high theoretical capacity of 660 mAh g^{-1}. However, the insertion of larger amount of Na ions into the structure always causes huge volume expansion, leading to continuous structural degradation and the gradual deterioration of electrochemical performance. The main challenges for sodium-alloy-based SIFCs are to suppress the volume change and maintain the electronic conduction during Na^+ insertion/deinsertion.

The construction of unique nanostructure is proved to be a resultful strategy to promote the electrochemical performance. A performance-oriented electrode structure with highly ordered 1D Sb nanorod arrays, good vertical alignment, and large interval spacing has been reported (**Figure 11**a,b).[21] This anode is able to serve as the additive and binder-free electrode, and exhibits a high specific capacity of 620 mAh g^{-1} with a retention of 84% after 250 cycles at 0.2 A g^{-1} in a sodium half-cell. A full cell assembled with a P2-$Na_{2/3}Ni_{1/3}Mn_{2/3}O_2$ cathode using 1.0 M $NaClO_4$- in EC-PC-5% FEC electrolyte was also constructed, and displayed an average operating voltage of 2.8 V, excellent cycling stability (250 cycles), high rate capability (20 A g^{-1}), and high energy density up to 130 Wh kg^{-1} (based on the total mass of anode and cathode) (Figure 11c). Other Sn nanopillars coated with carbon nanotubes which grow on the carbon paper have also been developed through a facile soaking–chemical-vapor deposition method.[149] This unique, free-standing electrode with a unique, 3D hierarchical architecture (Figure 11d) is able to provide a reversible capacity of 887 μA h cm^{-2} with good cyclability extending to 100 cycles. An SIFC with a lithium-substituted layered $Na_{0.80}Li_{0.12}Ni_{0.22}Mn_{0.66}O_2$ as a cathode (Figure 11e) is revealed to deliver a high operating voltage of 3.3 V with a capacity retention of 70% after 40 cycles (Figure 11f).

Another promising strategy is carbon decoration, where metal composites can be coated with a carbon shell or embedded into a carbon matrix. Chen's group[150] utilized Sn nanodots (size of 1–2 nm) finely encapsulated in porous, N-doped carbon nanofibers via the electrospinning method and subsequent pyrolyzation process. The obtained nanofibers with free-standing membrane can be directly used as binder- and current-collector-free anode, which delivers the capacity of 450 mAh g^{-1}, even at 10 000 mA g^{-1} and 483 mAh g^{-1} after 1300 cycles at 2000 mA g^{-1} in half-cell. The $NaVPO_4F$//Sn full cell has been constructed with the weight ratio of cathode to anode of 5.5:1. The full cell exhibits an initial capacity of ≈540 mAh g^{-1} (based on the mass of anode) with a good capacity retention of 85.2% after 100 cycles. Flexible power sources are proved to be available in next-generation implantable and wearable electronic systems. A soft-package SIFC consisted of flexible and binder-free $Na_3V_2(PO_4)_3$/rGO cathode and a Sb/rGO anode has been fabricated (Figure 11g,h).[151] Particularly, the porous, conductive, interconnected graphene frameworks, which allow the incorporation of Sb or $Na_3V_2(PO_4)_3$ nanocrystals, can maintain the integrity of electrical connectivity and reduce

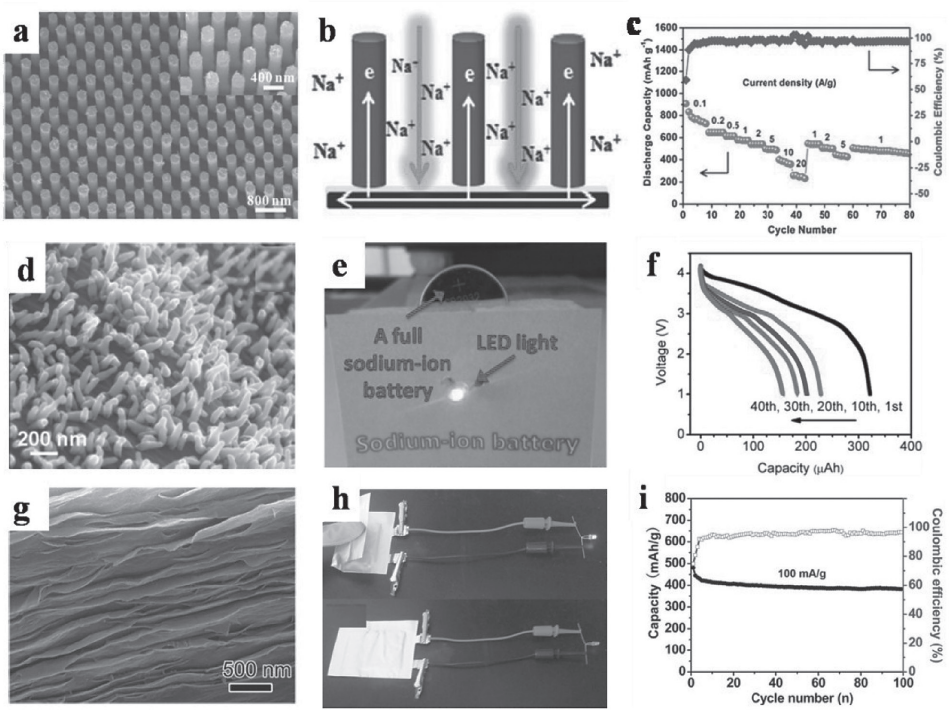

Figure 11. a) SEM image of the Sb nanorod arrays. b) The schematic illustration of the transport mechanism of Na ions and electrons in S-Sb NRs. c) Rate capability of a full cell coupled by a P2-$Na_{2/3}Ni_{1/3}Mn_{2/3}O_2$ cathode and a Sb-nanorod-array anode. Reproduced with permission.[21] Copyright 2015, The Royal Society of Chemistry. d) SEM image of Sn@CNT-CP with a hierarchical structure. e) An LED bulb is driven by the $Na_{0.80}Li_{0.12}Ni_{0.22}Mn_{0.66}O_2$//Sn@CNT-CP full cell. f) Discharge curves of the full cell. Reproduced with permission.[149] Copyright 2015, Elsevier. g) SEM image for the cross-section of the as-fabricated Sb/rGO paper. h) Digital pictures for the bending/free-bending NVP/rGO//Sb/rGO sodium-ion full cell that lights an LED. i) Long-term cycling performance and Coulombic efficiency of the NVP/rGO//Sb/rGO full cell. Reproduced with permission.[151] Copyright 2015, Wiley–VCH.

volume change during the Na^+ insertion/deinsertion processes. The $Na_3V_2(PO_4)_3$//Sb full cell is able of delivering a highly specific capacity of 400 mAh g^{-1} after 100 cycles at a current density of 100 mA g^{-1} (Figure 11i). Moreover, a nanostructured tellurium@carbon (nano-Te@C) composite by confining Te molecules in the space of carbon micropores has been synthesized.[152] The nano-Te@C is able to deliver a high capacity of 410 mAh g^{-1} with superior long-term cycling stability of 90% capacity retention over 1000 cycles. The practical feasibility of the nano-Te@C as an anode in SIFCs has been investigated through coupling with a $Na_{2/3}Ni_{1/3}Mn_{2/3}O_2$ cathode electrode, and the mass ratio for the two electrodes (anode/cathode) is 1:3. The $Na_{2/3}Ni_{1/3}Mn_{2/3}O_2$///Te full cell shows a high reversible capacity of 400 and 334 mAh g^{-1} at 0.1 and 0.5 C, respectively. It also demonstrates a good cycling performance of 95% capacity retention after 150 cycles, with the capacity maintained at 317 mAh g^{-1}. This is attributed to the resulting carbon decoration, which provides a buffer to suppress the volume change and structural aggregation of the metal during the insertion/deinsertion processes.

It is widely acknowledged that the construction of a hybrid-alloy phase is a valid method to improve the structural stability, since two different metal phases can operate as mutual buffers with each other to reduce the volume change.[153] A simple and inexpensive colloidal method is developed to synthesize the SnSb nanocrystals, and it has been used as both lithium- and sodium-ion anode materials.[154] Full cells are also constructed with $LiCoO_2$ and $Na_{1.5}VPF_{0.7}$ cathodes, realizing specific capacities of 600 and 400 mAh g^{-1} (based on the anode weight) with an average operating voltage of 3.0 and 2.7 V for lithium- and sodium-ions, respectively. As another candidate of Sb-based alloys, Mo_3Sb_7 has attracted great attention due to its excellent rate capability.[155] The electrochemical performance has been dramatically improved through the buffer effect of Mo component associated with the uniform carbon coating. The $Na_3V_2(PO_4)_3$//Mo_3Sb_7 full cell is able to deliver a capacity of ≈320 mAh g^{-1} at 0.2 A g^{-1}. However, the full cell just delivers an output voltage of 2.0 V, which is much lower than its theoretical value (3.0 V), and the polarization mechanism remains to be further investigated. Surface modification with TiO_{2-x} is a commendable method to synthesize the sodium-alloy materials. Wang et al.[156] reported double-walled crystalline Sb@TiO_{2-x} nanotubes obtained by the calcination of Sb_2S_3@TiO_2 nanorods in Ar/H_2. This material takes the advantages of excellent electrochemical stability of TiO_{2-x} and high capacity of Sb, together with its nanosize and hollow structure. When evaluated as an $Na_3V_2(PO_4)_3$//Sb@TiO_{2-x} full cell, it exhibits a high energy density of 151 Wh kg^{-1} at 21 W kg^{-1}, and 61 Wh kg^{-1} at 1.83 kW kg^{-1}.

In short, there are a series of approaches to suppress the volume change of alloy materials during Na ions insertion/deinsertion, including morphological construction, carbon decoration, alloying with different metals, and surface

modification, etc. Notably, the cycle life and energy density of alloy-based SIFCs exhibit great competitiveness with regard to carbon-based SIFCs. To develop the alloy-based SIFCs with promoted operating voltage and extended cycle-life in a cheap way has become a major challenge.

4.3. Metal-Oxides-Based SIFCs

Since $Li_4Ti_5O_{12}$ has been successfully commercialized in LIBs, metal oxides have attracted great attentions as expected in SIFCs.[157,158] Among various metal oxides, Ti-based electrodes are widely recognized as potential anode materials due to the low cost, high safety, low strain, and excellent structural stability during the insertion/extraction of sodium ions. However, Ti-based anode materials provide relatively low specific capacity and high operating voltage, resulting in low energy density. Therefore, the major prospect for Ti-based SIFCs focus on long-life, high-power, and high-safety energy storage applications.[159]

The spinel $Li_4Ti_5O_{12}$ is a well-known 'zero-strain' anode for LIBs,[160] and is able to be used as sodium electrode materials, which exhibits an average voltage of 0.91V with distinguished cycling stability. Sun et al.[161] initially reported a three-phase separation reaction of $Li_4Ti_5O_{12}$ with a reversible capacity of 155 mAh g^{-1} when use the high tensile-strength binder of carboxymethyl-cellulose (CMC). The $Na_3V_2(PO_4)_3$//$Li_4Ti_5O_{12}$ full cell gives rise to an average operating voltage plateau at ≈2.4 V with moderate rate and cyclic performance. Although TiO_2 has obtained great attentions as a versatile material used in numerous important technological areas, its applications as SIFCs anodes still remain insufficient. An all-oxide SIFC using an amorphous TiO_2-nanotube anode coupled with the $Na_{1.0}Li_{0.2}Ni_{0.25}Mn_{0.75}O_\delta$ cathode has been fabricated by Xiong et al.[162] for the first time, which shows good rate capability. $Na_2Ti_3O_7$ has a theoretical capacity of 310 mAh g^{-1} with a low operating voltage, which leads to a higher energy density in practical SIFCs. Ni et al.[20] reported surface engineered $Na_2Ti_3O_7$ nanotube arrays directly grown on Ti substrates (**Figure 12**a,b), which delivered specific capacities of 280 mAh g^{-1} and a superior cycling stability (over 10 000 cycles) as well as high rate capability (78 mAh g^{-1} at 10 C). The $Na_{2/3}(Ni_{1/3}Mn_{2/3})O_2$// $Na_2Ti_3O_7$ full cell has been assembled with a mass ratio of 3.5:1 after presodiation of the anode. The full cell delivers an average potential of 2.7 V and an energy density of 110 Wh kg^{-1} (based on the total mass of anode and cathode) with enhanced cycling stability (Figure 12c). $Na_2Ti_6O_{13}$ has been reported to be a safe anode with a plateau around 0.8 V. However, the specific capacity of the $Na_2Ti_6O_{13}$-based full cell is proved to be very low, thus seriously limiting its development.[163] Li substitution with transition metals has been considered as an effective way to improve the electrochemical performance. Wang et al.[164] reported a zero-strain,

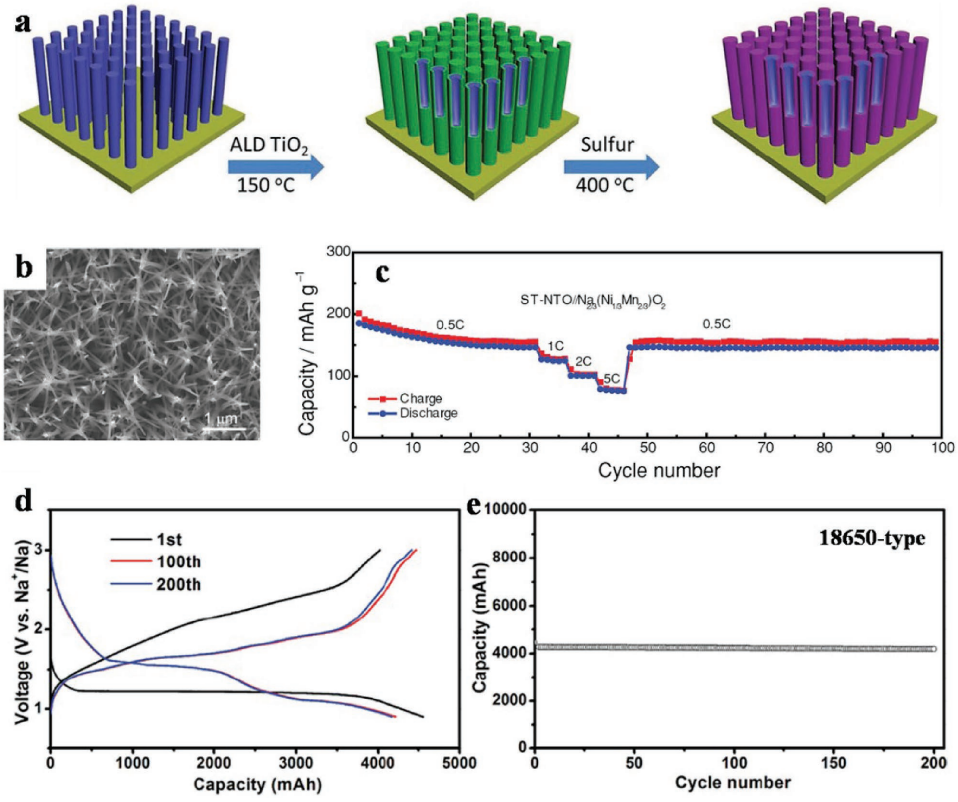

Figure 12. a) Schematic illustration of the fabrication of surface engineered $Na_2Ti_3O_7$ nanotube arrays grown on Ti foil. b) Top view of ST-NTO. c) Cycling performance of the $Na_{2/3}(Ni_{1/3}Mn_{2/3})O_2$//ST-NTO full cell upon various current rates. Reproduced with permission.[20] Copyright 2016, Wiley–VCH. d) Charge–discharge curves and e) cycling performance of a 18650-type battery at a current density of 4 A in the voltage range from 0.9-3 V. Reproduced with permission.[170] Copyright 2015, Royal Society of Chemistry.

layered P2-$Na_{0.66}[Li_{0.22}Ti_{0.78}]O_2$ anode material, which displays an average output voltage of 0.75 V, a specific capacity of 116 mAh g^{-1}, and extended cycling performance (75% capacity retention over 1200 cycles). Nevertheless, the operating voltage and cycling performance of the $Na_3V_2(PO_4)_3$//$Na_{0.66}[Li_{0.22}Ti_{0.78}]O_2$ full cell still need to be promoted.

Other metal oxides have been explored to deliver high capacity during sodium storage through the conversion reaction: $M_xO_y + 2yNa^+ + 2ye^- \leftrightarrow xM + yNa_2O$, (M = transition metal). Fe-based oxides are recognized as a low-cost candidate for Na-ion batteries, and the electrochemical properties of Fe_3O_4 nanoparticles synthesized through a simple hydrothermal method are investigated as an anode material for sodium half- and full cells.[165] The Fe_3O_4 with alginate binder delivers a reversible capacity of 248 mAh g^{-1} after 50 cycles at 0.1 C (half-cell). When extended to SIFCs, the $Na_3V_2(PO_4)_3$//Fe_3O_4 full cell displays an average voltage of 1.6 V with insufficient cycling performance. The practical energy density and cyclability of a full cell should be promoted by optimizing other parameters including electrode formula, cell balance, electrolytes, etc. Another all-Fe-based $Na_xFeFe(CN)_6$//FeO_x full cell has been reported by Li's group.[166] The carbon nanotubes supported ultra-small, poorly crystalline FeO_x nanoparticles show excellent cycling stability and rate performance in a half-cell. Notably, the $Na_xFeFe(CN)_6$//FeO_x full cell exhibits prolonged cycle-life over 400 cycles with Coulombic efficiency reaching close to 100% during the whole processes.

As a new type of oxide, α-MoO_3 has been reported as the anode material for SIFCs,[167] and it demonstrates sodiation and desodiation capacities of 771 and 410 mAh g^{-1} in the first cycle (initial Coulombic efficiency of 53.2%). The average discharge voltages of the sodium half-cell and $Na_3V_2(PO_4)_3$//MoO_3 full cell are about 0.5 V and 1.2 V, respectively, indicating high polarization of full cell. V-based materials are of particular interest owing to the various oxidation states accessible, achieving multielectron redox reactions. The amorphous V_2O_5 aerogel as anode material is able to deliver a capacity over 200 mAh g^{-1}. When evaluated as $Na_3V_2(PO_4)_3$//V_2O_5, the full cell displays a capacity of 113 mAh g^{-1} and 60 mAh g^{-1} based on the anode and the cathode, respectively. The capacity retention of the full cell reaches to 52% after 150 cycles with respect to the maximum value obtained in the 28th cycle.[157]

In short, although oxide-based anode materials have been extensively investigated in sodium half-cell with good electrochemical performance, their application in SIFCs still remains insufficient and unsatisfactory. Among them, $Na_2Ti_3O_7$ and Fe-based SIFCs provide the most promising reversible capacities with relatively good cycling stability. However, their relatively low initial Coulombic efficiency holds back the assembly of full cells and lowers the energy density due to the irreversible reaction. Some resultful strategies have been introduced to improve their initial Coulombic efficiency, including surface engineering, additives, and presodiation.

4.4. Others

Metal sulfides are always investigated as an anode materials for SIFCs with the reaction in two steps, that is, intercalation and conversion.[168] Similar to oxide-based anode materials, these sulfides usually suffer from large volume expansion and sluggish kinetics for Na^+ insertion/deinsertion during the chemical reaction. A series of approaches have been applied to solve these problems, such as structural construction, carbon decoration, and tuning the operating potential.[169] Chen's group[170] demonstrated the FeS_2 microspheres with only the intercalation reaction through the combined use of a compatible $NaSO_3CF_3$/diglyme electrolyte and controlling the cut-off voltage to 0.8 V. The FeS_2 half-cell exhibits an outstanding long-term cyclability (90% capacity retention for 20 000 cycles) and high-rate capability (170 mAh g^{-1} at 20 A g^{-1}), which is attributed to the formation of a stable, electrically-conductive, layer structured Na_xFeS_2. Notably, 18650-type sodium batteries are fabricated through commercial FeS_2 and Na foil, and display a high capacity of 4200 mAh (corresponding to 126 Wh kg^{-1}) with a capacity retention of 97% after 200 cycles at 4 A (Figure 12d,e). Similarly, the $FeSe_2$ anode has also been proved to deliver excellent cycling stability and good rate performance in both sodium half- and full cell.[171] CoS has been studied as potential anode material considering its high capacity and good electric conductivity. The CoS@rGO half-cell exhibits high specific capacity of 636 mAh g^{-1}, superior rate capability (306 mAh g^{-1} at 10 A g^{-1}), and ultralong cycle-life (420 mAh g^{-1} at 1 A g^{-1} after 1000 cycles). The further assembled $Na_3V_2(PO_4)_3$//CoS full cell displays initial charge and discharge capacities of 498 and 381 mAh g^{-1} (based on the mass of anode) with 75% capacity retention after 100 cycles.[172] As a typical layered metal sulfide, SnS_2 has a layered structure consisting of tin atoms sandwiched between two layers of hexagonal close-packed sulfur atoms, which offers a large interlayer spacing for Na^+ insertion/extraction.[173] Although the SnS_2-RGO hybrid structure shows good performance in half-cell, its cycling stability and initial Coulombic efficiency remain unsatisfactory for $Na_{0.80}Li_{0.12}Ni_{0.22}Mn_{0.66}O_2$//$SnS_2$ full cell.[174] Other metal-sulfides-based SIFCs have also been investigated, including $Na_{2/3}Ni_{1/3}Mn_{2/3}O_2$//$Sb_2S_3$,[175] $NaVPO_4F$//WS_2,[176] $Na_3V_2(PO_4)_2F_3$//SnS,[177] $Na_3V_2O_{2x}(PO_4)_2F_{3-2x}$//$MoS_2$,[178] and $Na_3V_2(PO_4)_3$//Bi_2S_3.[179]

Organic electrode materials have been testified to be potential anode electrodes due to the following merits: low-cost, structural flexibility, and possible multielectron reactions. Abouimrane et al.[180] reported sodium insertion in a series of organic carboxylate-based materials at low voltage, and the $C_8H_5NaO_4$/Na cell exhibits good cycling performance with more than 226 mAh g^{-1} after 50 cycles at a current density of 40 mA g^{-1}. In this contribution, 3.6 V SIFCs using these organic anodes and an $Na_{0.75}Mn_{0.7}Ni_{0.23}O_2$ cathode have been successfully constructed with good cycling performance. Another polyimide is found to deliver a specific capacity of 140 mAh g^{-1} and still maintains 60% of the capacity even at 32 C.[121] The $Na_4Fe(CN)_6$//polyimide full cell also exhibits a high capacity of about 140 mAh g^{-1}, based on the anode with relatively low operating voltage of 1.1 V. Other potential organic anode-based SIFCs have also been investigated, including polyimide//disodium-terephthalate,[122] NVP//Juglone,[119] $Na_4C_8H_2O_6$//$Na_4C_8H_2O_6$,[118] and polytriphenylamine//poly(anthraquinonyl sulphide).[123]

Table 2. Electrochemical behaviors of anode-based SIFCs.

Anode	Cathode	Voltage (V)	Capacity (mA h g^{-1})	Capacity Retention	Initial CE of Anode
graphite[130]	$Na_{1.5}VPO_{4.8}F_{0.7}$	2.9	103 (500 mA g^{-1})	70% (250 cycles)	60%
graphite[133]	$Na_3V_2(PO_4)_3$	2.2	90 (200 mA g^{-1})	80% (400 cycles)	90%
hard carbon[138]	$NaNi_{0.5}Mn_{0.5}O_2$	2.8	240 (300 mA g^{-1})	61% (80 cycles)	90%
hard carbon[139]	$NaCrO_2$	2.8	260 (20 mA g^{-1})	≈100% (5 cycles)	78%
hard carbon[141]	$Na_{2/3}Ni_{1/3}Mn_{2/3}O_2$	3.5	300 (0.1 C)	73% (150 cycles)	90%
hard carbon[142]	$Na_{0.9}Cu_{0.22}Fe_{0.30}Mn_{0.48}O_2$	3.2	240 (0.2 C)	97% (100 cycles)	80%
hard carbon[145]	$NaxNi_{0.22}Co_{0.11}Mn_{0.66}O_2$	2.4	250 (0.1 C)	81% (100 cycles)	70%
hard carbon[71]	$Na_{7/9}Cu_{2/9}Fe_{1/9}Mn_{2/3}O_2$	3.6	325 (0.2 C)	89% (50 cycles)	–
Sn@CNT[149]	$Na_{0.8}Li_{0.12}Ni_{0.22}Mn_{0.66}O_2$	3.3	–	70% (40 cycles)	73%
Sn@C[150]	$NaVPO_4F$	1.5	540 (500 mA g^{-1})	82% (100 cycles)	70%
Sb[21]	$Na_{2/3}Ni_{1/3}Mn_{2/3}O_2$	2.8	620 (500 mA g^{-1})	54% (250 cycles)	81%
SnSb[154]	$Na_{1.5}VPO_{4.8}F_{0.7}$	2.7	400 (200 mA g^{-1})	100% (60 cycles)	65%
Sb@TiO_{2-x}[156]	$Na_3V_2(PO_4)_3$	2.4	500 (660 mA g^{-1})	70% (100 cycles)	73%
Te@C[152]	$Na_{2/3}Ni_{1/3}Mn_{2/3}O_2$	2.0	400 (0.1 C)	95% (150 cycles)	61%
Mo_3Sb_7[155]	$Na_3V_2(PO_4)_3$	2.0	320 (200 mA g^{-1})	97% (20 cycles)	67%
TiO_2[162]	$NaLi_{0.2}Ni_{0.25}Mn_{0.75}O_\delta$	1.8	80 (11 mA g^{-1})	–	64%
$Li_4Ti_5O_{12}$[161]	$Na_3V_2(PO_4)_3$	2.4	135 (0.1 C)	90% (16 cycles)	81%
$Na_2Ti_6O_{13}$[163]	$Na_3V_2(PO_4)_2F_3$	2.7	42 (0.2 C)	93% (20 cycles)	78%
$Na_2Ti_3O_7$[20]	$Na_{2/3}Ni_{1/3}Mn_{2/3}O_2$	2.7	210 (0.2 C)	75% (100 cycles)	55%
$Na_{0.66}[Li_{0.22}Ti_{0.78}]O_2$[164]	$Na_3V_2(PO_4)_3$	2.6	90 (0.5 C)	87% (20 cycles)	74%
V_2O_5[157]	$Na_3V_2(PO_4)_3$	2.5	–	61% (200 cycles)	52%
SnS[177]	$Na_3V_2(PO_4)_2F_3$	2.4	330 (0.2 mA cm^{-2})	76% (100 cycles)	77%
SnS_2[174]	$Na_{0.80}Li_{0.12}Ni_{0.22}M_{0.66}O_2$	2.3	–	74% (50 cycles)	81%
SnS_2[173]	$Na_3V_2(PO_4)_3$	1.6	375 (100 mA g^{-1})	53% (12 cycles)	66%
MoS_2[178]	$Na_3V_2O_{2x}(PO_4)_2F_{3-2x}$	1.8	105 (13 mA g^{-1})	72% (40 cycles)	84%
Sb_2S_3[175]	$Na_{2/3}Ni_{1/3}Mn_{2/3}O_2$	2.2	–	97% (10 cycles)	67%
Bi_2S_3[179]	$Na_3V_2(PO_4)_3$	1.7	340 (100 mA g^{-1})	84% (6 cycles)	71%
CoS[172]	$Na_3V_2(PO_4)_3$	1.7	381 (500 mA g^{-1})	76% (100 cycles)	95%
WS_2[176]	$NaVPO_4F$	1.6	330 (100 mA g^{-1})	76% (20 cycles)	73%
$FeSe_2$[171]	$Na_3V_2(PO_4)_3$	1.7	366 (1000 mA g^{-1})	89% (200 cycles)	98%
$C_8H_5NaO_4$[180]	$Na_{0.75}Mn_{0.7}Ni_{0.23}O_2$	3.6	280 (40 mA g^{-1})	96% (50 cycles)	40%
polyimide[121]	$Na_3V_2(PO_4)_3$	1.1	150 (140 mA g^{-1})	65% (100 cycles)	98%
di-terephthalate[122]	polyimide	1.4	190 (50 mA g^{-1})	65% (20 cycles)	≈100%
black phosphorus[216]	$Na_{0.66}Ni_{0.26}Zn_{0.07}Mn_{0.67}O_2$	2.7	–	87% (100 cycles)	90%
Cu_3P[217]	$Na_3V_2(PO_4)_3$	2.7	209 (600 mA g^{-1})	38% (200 cycles)	≈65%

4.5. Comparisons of Anode-Based SIFCs

The electrochemical properties of the main anode-materials-based SIFCs have been further summarized. The detailed definitions of different parameters in **Table 2** are as follows: 1) "Voltage" represents the average operating voltage of the full cell; 2) the calculation of "Capacity" is based on the mass of anode active material; 3) "Initial C. E. of Anode" represents the initial Coulombic efficiency of the anode material in the half-cell. To begin with, graphite, which has been extensively used in commercial LIBs, shows negligible electrochemical activity with Na ions. Instead, carbonaceous, especially hard-carbon-based, SIFCs exhibit the highest operating potential up to 3.5 V, with discharge capacity of ≈325 mAh g^{-1}. These two parameters are significant and even close to the commercialized graphite, which endows it a promising anode for SIFCs. However, its rate capability as well as long-term cycling stability remains unsatisfactory due to the amorphous structure. Alloy-based SIFCs contribute high specific capacity of about 600 mAh g^{-1}, while the volume expansion during sodiation/desodiation is quite huge, which not only decreases the structural stability but also prevents it from practical application. The morphological construction, carbon decoration, and alloying with different metals

are the major approaches to solve this problem. Oxide-based SIFCs are in the initial stage of their investigation and exhibit low discharge capacity and moderate output voltage so far. Among them, Ti-based oxide materials have been investigated as host materials for SIFCs owing to their appropriate operation voltage, low cost, and eco-friendliness. To serve as a qualified anode material, the specific capacity of Ti-based oxide needs to be greatly enhanced. Metal-sulfides based SIFCs deliver a specific capacity of ≈400 mAh g^{-1}. Nevertheless, it provides a relatively low output voltage with poor cycling stability due to the large volume expansion and sluggish kinetics for Na^+ insertion/deinsertion during the chemical reaction. On the whole, the carbon-based materials, especially hard carbon, are currently the most promising anode for SIFCs owing to the low-cost and decent specific capacity.

5. Aqueous Sodium-Ion Full Cells

Concerns in terms of the 'green' quality of energy have long existed, and these issues have been addressed in a variety of approaches through the years.[181,182] Aqueous batteries have been selected as a preferable family owing to their low cost, abundant resources, and eco-friendliness. Therefore, a series of the rechargeable batteries choose water-based electrolytes, including Pb-acid, Ni-Cd, and Ni-MH.[183–185] Despite their cost advantages, these commercialized batteries are still troubled by the undesirable service life and heavy metal pollution. Under this background, the aqueous rechargeable alkali-ion batteries, which takes advantage of both water-based electrolyte and alkali-ion batteries, have attracted great attention.[186] On the one hand, the water-based solution is capable of delivering a higher specific conductivity (10^{-2}–10^{-1} S cm^{-1})[183] compared with organic electrolytes (10^{-3}–10^{-1} S cm^{-1}),[187] inorganic solid electrolytes (10^{-7}–10^{-2} S cm^{-1}),[188,189] and polymer electrolytes (10^{-7}–10^{-3} S cm^{-1}).[190,191] On the other hand, the reaction mechanism of alkali ion batteries with water-based electrolyte exhibits similar redox behavior as in organic-based electrolyte, enabling superior cycling stability during the intercalation reaction of alkali ions among electrode materials. Li et al.[192] firstly introduced the aqueous LIBs in 1994, which opened a new direction in the field of electrochemistry energy storage. However, the following explored electrode couples were not able to provide desirable cycling stability until the $LiTi_2(PO_4)_3$/$LiFePO_4$ aqueous Li-ion full cell developed by Xia's group.[193]

Compared with aqueous LIBs, the sodium-ion full cells with aqueous electrolyte can further decrease manufacture cost and eliminate the "voltage penalty" in organic electrolyte due to the limited operating voltage of H_2O (≈1.2 V). Therefore, aqueous SIFCs possess great potential to be utilized as a green, safe, and low-cost power source for grid-scale energy storage applications. The basic working condition of aqueous SIFCs depends on the intercalation of Na ions in water-based environment. Thus, it is important to choose suitable electrode couple with appropriate operating voltage to avoid water decomposition, as is shown in **Figure 13**. Although the theoretical stability window of water is about 1.2 V, the durable potential can be extended owing to the kinetic effect,[194,195] and other water-based batteries also display a higher output voltage, such as Pb-acid batteries. Up to now, the investigation of aqueous SIFCs is in the initial stage; however, the long-term cycling stability and high rate capability of the aqueous SIFCs have been greatly promoted, and these improvements have in turn attracted more attention for aqueous system investigations.

5.1. Electrode Materials of Aqueous SIFCs

The reaction process in the aqueous solution seems to be more complex compared to the reaction in the organic electrolyte, and many parameters should be taken into

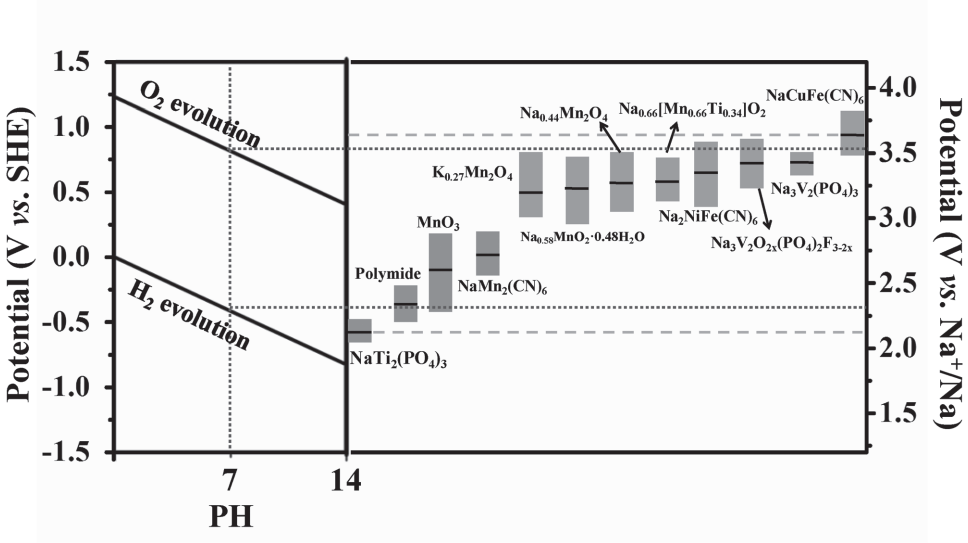

Figure 13. Stability potential window of selected electrode materials in aqueous solution.

consideration in cell assembly, such as dissolution of the metal ion, concentration of the electrolyte, pH of the solution, additives, dissolved oxygen, etc.[183] Furthermore, the limited electrode materials that are electrochemically active in aqueous electrolyte have also hindered the application of aqueous SIFCs. Therefore, exploring suitable electrode materials, which suppress the side reaction of the battery and show good adaptability, are of great importance. Different from non-aqueous SIFCs, the electrode materials that have been investigated for aqueous SIFCs are restricted, including polyanionic compounds, oxides, carbonaceous material, Prussian blue, and polymer.

Among various electrode materials, $NaTi_2(PO_4)_3$ has been considered as the most promising anode for aqueous SIFCs owing to the proper redox potential (–0.6 V vs SCE), high specific capacity (133 mAh g^{-1}), superior structural stability (NASICON), and excellent durability in deoxygenated water.[196] As for cathode, $Na_{0.44}MnO_2$ has attracted great attention owing to good cycling stability, proper charge/discharge voltage, ease of synthesis, and low-cost since the first report by Whitacre et al.[197] Therefore, the $Na_{0.44}MnO_2$//$NaTi_2(PO_4)_3$ are sought in aqueous SIFCs. As for the $NaTi_2(PO_4)_3$ anode, the main optimization strategy is to improve its intrinsic low electronic conductivity through carbon decoration, morphologic construction, and structural modification. A facile high energy ball-milling method has been developed to synthesize the pure phase NTP-C.[22] When coupled with an $Na_{0.44}MnO_2$ cathode, the $Na_{0.44}MnO_2$//$NaTi_2(PO_4)_3$ aqueous SIFC exhibits a high reversible capacity of about 120 mAh g^{-1} at 0.6 C (based on the mass of $NaTi_2(PO_4)_3$) in a three-electrode configuration. The full cell is also capable of delivering an ultrahigh rate capability of 270 C and long-term cycling stability over 1600 times. However, the larger polarization of the $NaTi_2(PO_4)_3$ anode than the $Na_{0.44}MnO_2$ cathode becomes the shortcoming for the full cell, which lower the energy density in high-power applications. To further promote the electronic conductivity and suppress the polarization of the $NaTi_2(PO_4)_3$ anode, a frogspawn-inspired hierarchical porous $NaTi_2(PO_4)_3$–C array material has been constructed.[198] The frogspawn-inspired $NaTi_2(PO_4)_3$-C array displays the lowest R_{ct} value and slowest increasing rate for the different potential state compared with control samples, leading to enhanced electrochemical behaviors. The $Na_{0.44}MnO_2$//$NaTi_2(PO_4)_3$ aqueous full cell has also been investigated and demonstrates excellent rate (≈20 mAh g^{-1} at 90 C) and cycling performance (≈70% capacity retention after 1000 cycles) based on the total mass of the active materials (**Figure 14**a,b). Besides, the carbon decoration method,[199] concentration of electrolyte,[200] effect of electrolyte additives,[201] and different electrode couples[202,203] have also been explored for optimizing NTP-based aqueous SIFCs.

As for tunnel-structured $Na_{0.44}MnO_2$ cathode, the main strategy is to improve its specific capacity since only half of the Na ions can be extracted, and further extraction would cause the O_2 evolution. To overcome this limitation, more and more $Na_{0.44}MnO_2$ ramifications-based aqueous SIFCs have been developed in order to promote the energy density and cycling stability of the system. One of the methods is to synthesize tunnel-type material with valence state of Mn lower than $Na_{0.44}MnO_2$ ($Mn^{3.56+}$), thus more sodium ions might be extracted and a higher capacity could be achieved. This is because the low redox reaction potential of Mn ions can avoid O_2 evolution. Qian's group[204] reported the $NaMnO_2$//$NaTi_2(PO_4)_3$ aqueous SIFC based on the facile solid-state reaction and sol–gel post heat-treatment method, respectively. The full cell demonstrates a sloping charge/discharge curve in the whole voltage range of 0.5 to 1.8 V. It also delivers an energy density of 30 W h kg^{-1} at a power density of 50 W kg^{-1} (based on the total mass of the active electrode materials) and retains 75% of the capacity after 500 cycles at a high rate of 5 C. To further improve the specific discharge capacity of the $Na_{0.44}MnO_2$ cathode, a Ti-substituted, sodium-rich, tunnel-type positive material ($Na_{0.66}[Mn_{0.66}Ti_{0.34}]O_2$) with higher discharge capacity has been developed.[205] It is noted that five different transition metal sites and three sodium sites are evidently distinguished in Figure 14c. The valence states of Mn/Ti can be deduced to Mn^{3+} and Ti^{4+} states, respectively. Particularly, it displays the high reversible capacity of about 76 mAh g^{-1} at a current rate of 2 C, with an average operating voltage of 1.2 V when assembled with NTP/C anode in aqueous SIFCs (Figure 14d). The dissolution of Mn from active materials has been proved in aqueous electrolyte, which is due to the polarity of water molecules and the lack of protection from solid-electrolyte interface, leading to the decay of capacity. The existence of crystal water in layered structure is able to enhance the structural stability. More recently, Na-birnessite $Na_{0.58}MnO_2{\cdot}0.48H_2O$ has been synthesized and it delivers a high reversible capacity of about 80 mAh g^{-1} at 1 C, with a 100% initial capacity retention after 1000 cycles at 10 C, which is superior to that without crystal water. The $Na_{0.58}MnO_2{\cdot}0.48H_2O$//$NaTi_2(PO_4)_3$ full cell also exhibits a highly stable cycling performance over 1000 cycles at 10 C with only a 5.8% capacity loss, and it delivers a high reversible capacity of 50 mAh g^{-1} at 1 C based on the total mass of the active materials.

As another type chemical stability electrode materials in H_2O, Prussian blue analogues have also been studied as potential alternatives for aqueous SIFCs owing to the open-framework structure with large channels and interstices, which allows the fast insertion and extraction of Na ions with little lattice strain.[206] Besides, the specific capacity and operating voltage can be maximized through the proper selection of transition-metal cations at the M site in the Prussian blue compounds ($Na_xM_yFe(CN)_6$, M = Fe, Co, Cu, Ni, etc.). Wu et al.[207] reported an aqueous SIFC based on Na-rich $Na_2NiFe(CN)_6$ cathode, Na-deficient $NaTi_2(PO_4)_3$ anode, and 1 M Na_2SO_4 solution (pH = 7) purged with N_2 as electrolyte. The $Na_2NiFe(CN)_6$ cathode displays quite similar charge/discharge profiles with well-defined voltage plateaus at 0.4–0.6 V (V vs Ag/AgCl) and delivers discharge capacity of 65 mAh g^{-1} at 1 C. Notably, the $Na_2NiFe(CN)_6$//$NaTi_2(PO_4)_3$ aqueous SIFC exhibits very good cycling stability with 88% capacity retention after 250 cycles at 5 C. The full cell also demonstrates a specific energy of 42.5 Wh kg^{-1} at a power density of 130 W kg^{-1}, and still remains 34 Wh kg^{-1} at a high power of 1200 W kg^{-1} (based on the total mass of active materials). Cui's group[208] developed a full open-framework

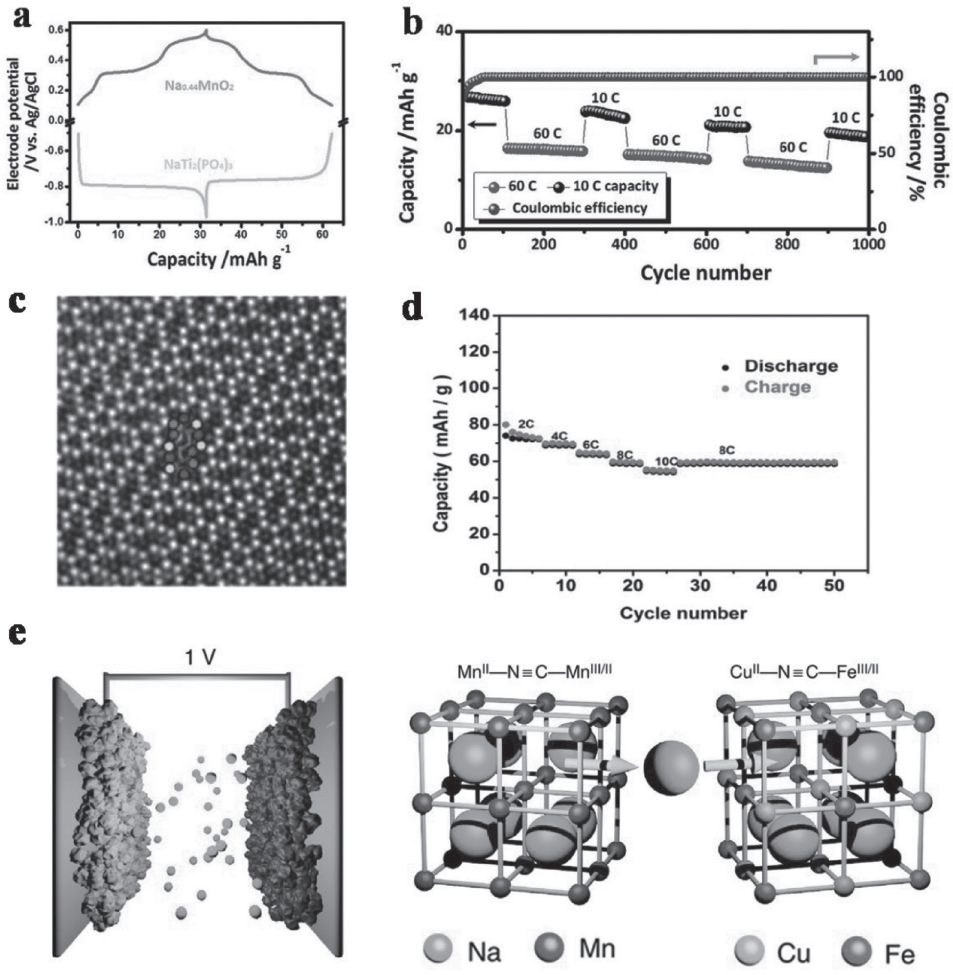

Figure 14. a) Charge/discharge curves of individual $Na_{0.44}MnO_2$ cathode and frogspawn-inspired $NaTi_2(PO_4)_3$ anode. b) Long-term cycling performance of the full cell at alternate 10 and 60 C for one thousand cycles. Reproduced with permission.[198] Copyright 2015, The Royal Society of Chemistry. c) STEM image of general view of the crystal structure and view along [001]-zone axis. d) Rate performance of $Na_{0.66}[Mn_{0.66}Ti_{0.34}]O_2$//$NaTi_2(PO_4)_3$/C full cell cycled in the voltage range of 0.3–1.7 V at various current rates. Reproduced with permission.[205] Copyright 2015, Wiley–VCH. e) Symmetric open-framework cell schematic. Reproduced with permission.[208] Copyright 2014, Macmillan Publishers Limited.

aqueous battery based on manganese hexacyanomanganate anode and copper hexacyanoferrate cathode (Figure 14e). The full cell exhibits no measurable capacity loss after 1000 cycles at 10 C with Coulombic efficiency reaching up to 99.8% during cycling. This symmetric battery delivers a maximum specific energy of 27 Wh kg^{-1} at 1 C and maintains 84.2% energy efficiency when cycled at 50 C based on the mass of the active materials.

Polyanionic compounds have been dramatically explored as promising electrode materials in non-aqueous full cells in recent years. These materials exhibit excellent structural stability with an open framework structure that benefits for the diffusion of alkali ions. It also possesses relatively high operating potentials owing to the inductive effect which may endow it as suitable electrode materials for aqueous battery systems. The reversible electrochemical reaction of the $Na_3V_2O_{2x}(PO_4)_2F_{3-2x}$ with multiwalled carbon-nanotubes in concentrated aqueous solution (10 M $NaClO_4$) is firstly reported by Kim's group.[209] When evaluated as $Na_3V_2O_{2x}(PO_4)_2F_{3-2x}$//$NaTi_2(PO_4)_3$ SIFCs, the full cell exhibits a discharge capacity of 30 mAh g^{-1} (based on the mass of cathode) after 400 cycles at a high rate of 10 C (corresponding to 75% capacity retention). Obviously, the energy density of $Na_3V_2O_{2x}(PO_4)_2F_{3-2x}$//$NaTi_2(PO_4)_3$ is unsatisfied and more cathode material with higher specific capacity is required. Among series polyanionic materials, olivine $NaFePO_4$ possesses the highest theoretical capacity (154 mAh g^{-1}) with operating voltage about 2.9 V vs Na^+/Na, and has been investigated to deliver a high specific capacity of 110 mAh g^{-1} at C/10 and 74 mAh g^{-1} at 2 C when tested at 55 °C in aqueous electrolyte. The $NaFePO_4$//$NaTi_2(PO_4)_3$ aqueous full cell exhibits an initial capacity of 70 mAh g^{-1} and a capacity retention of 76% after 20 cycles with an average operating voltage of 0.6 V.[210] To further promote the operating voltage of the aqueous SIFCs, the prototype $Na_3V_2(PO_4)_3$//$NaTi_2(PO_4)_3$ full cell with an average operating potential of 1.2 V has been conducted. The energy density of the full cell is calculated to be 36 Wh kg^{-1} at a power density of 2567 W kg^{-1}, and still retains on 29 Wh kg^{-1} at 5145 W kg^{-1} (based on the total mass of active materials).

Table 3. Electrochemical behaviors of electrodes-based aqueous SIFCs.

Type	Cathode	Anode	Voltage (V)	Capacity (mA h g^{-1})	Capacity Retention
Cathode-based					
Mn-based oxides	$Na_{0.44}MnO_2$[197]	Active carbon	0.9	45 (1/8 C)	≈100% (1000 cycles)
	$NaMnO_2$[204]	$NaTi_2(PO_4)_3$	0.9	50 (1 C)	75% (500 cycles)
	$Na_{0.58}MnO_2{\cdot}0.48H_2O$[218]	$NaTi_2(PO_4)_3$	1.4	79 (1 C)	94% (1000 cycles)
	$Na_{0.66}[Mn_{0.66}Ti_{0.34}]O_2$[205]	$NaTi_2(PO_4)_3$	1.2	76 (2 C)	89% (300 cycles)
	$K_{0.27}MnO_2$[203]	$NaTi_2(PO_4)_3$	0.8	70 (150 mA g^{-1})	≈100% (100 cycles)
	$K_{0.27}MnO_2$[219]	$NaTi_2(PO_4)_3$	0.7	83 (200 mA g^{-1})	83% (100 cycles)
	A-δ-MnO_2[220]	$NaTi_2(PO_4)_3$	0.8	66 (200 mA g^{-1})	90% (200 cycles)
Prussian blue analogues	$Na_2CoFe(CN)_6$[221]	$NaTi_2(PO_4)_3$	1.5	100 (5 C)	98% (100 cycles)
	$Cu^{II}—N{\equiv}C—Fe^{III/II}$ [208]	$Mn^{II}—N{\equiv}C—Mn^{III/II}$	1.0	–	≈100% (1000 cycles)
	$KCo_{0.5}Cu_{0.5}Fe(CN)_6$[222]	SNDI	0.9	34 (10 C)	88% (100 cycles)
Polyanionic compounds	$NaFePO_4$[210]	$NaTi_2(PO_4)_3$	0.6	70 (1 C)	76% (20 cycles)
	$NaFe_{0.95}V_{0.05}PO_4$[223]	$Na_{1.2}V_3O_8$	0.5	100 (100 mA g^{-1})	90% (1000 cycles)
	$Na_3V_2(PO_4)_3$[224]	$NaTi_2(PO_4)_3$	1.2	62 (1000 mA g^{-1})	50% (50 cycles)
	$Na_3V_2O_{2x}(PO_4)_2F_{3-2x}$[209]	$NaTi_2(PO_4)_3$	1.5	39 (10 C)	75% (400 cycles)
	$Na_3V_2O_{2x}(PO_4)_2F_{3-2x}$[201]	$NaTi_2(PO_4)_3$	1.5	39 (10 C)	90% (200 cycles)
Anode-based					
$NaTi_2(PO_4)_3$	$Na_{0.44}MnO_2$	$NaTi_2(PO_4)_3$[199]	0.9	130 (0.1 C)	86% (100 cycles)
	$Na_{0.44}MnO_2$	$NaTi_2(PO_4)_3$[198]	1.1	112 (0.5 C)	84% (500 cycles)
	$Na_{0.44}MnO_2$	$NaTi_2(PO_4)_3$[225]	0.9	68 (16 mA g^{-1})	78% (20 cycles)
	$Na_{0.44}MnO_2$	$NaTi_2(PO_4)_3$[22]	1.1	103 (3 C)	50% (1600 cycles)
	$Na_{0.44}MnO_2$	$NaTi_2(PO_4)_3$[200]	0.9	110 (0.1 C)	–
	$Na_2NiFe(CN)_6$	$NaTi_2(PO_4)_3$[207]	1.3	100 (1 C)	88% (250 cycles)
	$Na_2CuFe(CN)_6$	$NaTi_2(PO_4)_3$[206]	1.4	104 (2 C)	88% (1000 cycles)
	$FePO_4$	$NaTi_2(PO_4)_3$[202]	0.7	100 (0.2 mA)	60% (20 cycles)
Oxides	$Na_{0.35}MnO_2$	MoO_3[226]	0.8	25 (550 mA g^{-1})	79% (1000 cycles)
	$Na_{0.44}MnO_2$	$Na_2V_6O_{16}{\cdot}nH_2O$[227]	0.9	30 (40 mA g^{-1})	77% (30 cycles)
Organics	$NaVPO_4F$	Polymide[228]	1.0	165 (50 mA g^{-1})	68% (20 cycles)

5.2. Comparisons of Electrode-Materials-Based Aqueous SIFCs

To systematically compare the electrochemical properties of the major current families of electrode materials for aqueous SIFCs, we categorize their average operating voltages, specific capacities, and cycling performance in **Table 3**. "Capacity" represents the specific capacity of the electrode material in the full cell, which is based on the mass of cathode (cathode-based) or anode (anode-based). Among cathode-based aqueous SIFCs, Mn-based oxides exhibit excellent cycling stability over 1000 times. However, the specific discharge capacity of Mn-based oxides is relatively low due to the limited utilization of Na ions, resulting in low energy density. Exploring novel Mn-based ramification is a valid way to improve its energy density. Prussian blue-based aqueous SIFCs are able to deliver a high discharge capacity of 100 mAh g^{-1} with the operating voltage up to 1.5 V. Further investigations should pay more attention to promote their structural stability as well as initial Coulombic efficiency. Polyanionic-compounds-based aqueous SIFCs provide a wide distribution of operating potential and specific capacity owing to its structural diversity. The energy density has been restricted by its relatively low specific capacity owing to poor reaction kinetics or a large molecular weight. $NaTi_2(PO_4)_3$-anode-based aqueous SIFCs display proper output voltage (≈1.2 V), long-term cyclability (over 1000 times), acceptable reversible capacity (≈130 mAh g^{-1}), and superior adaptability, which makes it to be the most attractive anode material for aqueous batteries. However, the relatively low theoretical capacity of $NaTi_2(PO_4)_3$ becomes the short slab for achieving high energy-density. Other types of anode material with higher specific capacity, such as organics, should be further investigated. All in all, aqueous SIFCs have aroused great interest for grid-system application as they are much cheaper, greener, and safer than the conventional LIBs with organic electrolyte. Although high-efficiency and long-life aqueous SIFCs for high power applications might be achieved, the undesirable reversible capacity of the electrode material and low operating voltage keep it a long way to go before the practical application.

6. Conclusions and Perspectives

Through systematically summarizing the most recent discoveries, technological developments, and major challenges of electrode-based SIFCs, this Review aims to present new insight into the understanding of full cells and lay a solid foundation for building advanced batteries. Although the energy density of SIFCs may be inferior to LIBs due to the large atomic weight and higher potential (0.33 V vs Li) of Na ions, their cost per energy and cost per lifetime are capable of compensating these limitations, especially for large-grid applications. The Na-contained precursors for electrode materials and electrolyte in SIFCs are basically cheaper than those for LIBs, and the replacement of inexpensive and lighter Al instead of Cu as a current collector is beneficial to realizing low-cost and high specific-gravimetric energy. It is anticipated that the industrialization of cost-effective SIBs as a substitute for LIBs may start in the near future, even though various challenges still exist. Thus, the investigation towards SIFCs is of great significance since it acts as the bridge in connecting the sodium half-cell and practical batteries.

(i) *Cathode materials*. Specific capacity, operating potential as well as tap density are the uppermost indexes in material investigation, which influence the specific gravimetric/volumetric energy of the full cell to a great extent. Layered oxides have been considered as the most promising candidates for SIFCs owing to the high specific capacity. To further achieve high energy density, the operating potential of the layered oxides should be promoted via proper cationic doping or substitution. It is, however, still necessary to improve the cycling stability during the deep insertion/deinsertion of Na ions. Polyanionic compounds are capable of delivering superior cycling stability as well as high output voltage because of the open framework structure and the inductive effect of the anions. However, the heavy polyanionic group leads to the relatively low specific capacity, which limits the total energy density of the full cell. Exploring suitable carbon decoration method along with the modification of the polyanionic groups is currently the major subject to optimize their electrochemical performance in terms of energy density, rate capability, and cycle life.

(ii) *Anode materials.* Compared to graphite, disordered carbon with a large interlayer distance exhibits a reversible capacity of 300 mAh g^{-1} and an average operating potential of ≈0.1 V. Nevertheless, its rate capability and cycling stability still require to be promoted. In terms of the cost, technological developments, and overall electrochemical performance, carbonaceous materials especially disordered carbon possess the greatest potential for future application. Most importantly, the majority of anode materials suffer from intrinsic low initial CE due to the SEI formation, which consumes the limited sodium resources in full cell. The further understanding of the reaction mechanism between electrode and electrolyte is of great significance. The simple and scalable presodiation method, which is able to offset the consumption of Na ions during the SEI formation, is urgently needed for practical applications.

(iii) *Aqueous SIFCs*. Concerns regarding the 'green' quality of batteries are more aware than ever and have been addressed in a variety of ways over the years. Aqueous SIFCs have emerged as the environmental friendliness, low-cost, and high-security devices for ESS. It can further reduce the cost and eliminate "voltage penalty" compared with organic electrolyte due to the limited operating voltage of H_2O (≈1.2 V). The ion conductivity of aqueous solution is much higher than that of non-aqueous electrolyte, resulting in high-rate and high-power capability. Through optimizing the electrode design, pH of the electrolyte, dissolved oxygen, and battery-assembly technologies, the aqueous SIFCs may exhibit prolonged cycling-life and superior rate capability in comparison with other secondary batteries. Among various electrode materials, Na_xMnO_2 cathode and $NaTi_2(PO_4)_3$ anode are the most widely studied candidates for aqueous SIFCs. However, the application of aqueous SIFCs still has a long way to go due to the low specific capacity and limited output voltage, which is currently the most significant barrier.

Overall, the electrochemical performance of SIFCs follows the "Cannikin Law", and their developments are basically based on the integrated progress of cathode, anode, separator and electrolyte, which indicates that a high rate capability cathode combined with a low rate capability anode does not make sense. SIBs are able to compete with LIBs in several important aspects, but the immature technology of SIFCs holds back their practical application. Therefore, the model of SIFCs should be further built and understood with consideration of both similarity and difference to LIBs. It is noted that cost issues and sustainable technologies always lie on the primary consideration for the future SIFCs.

Acknowledgements

W.R. and Z.Z. contributed equally to this work. This work was supported by the National Key Research and Development Program of China (2016YFA0202603), the National Basic Research Program of China (2013CB934103), the National Natural Science Foundation of China (51521001, 51602239), the National Natural Science Fund for Distinguished Young Scholars (51425204), and the Fundamental Research Funds for the Central Universities (WUT: 2016III001, 2016-KF-2, 2016III003, 2016IVA090). L.M. acknowledge the scholarship from the China Scholarship Council.

[1] D. Larcher, J. M. Tarascon, *Nat. Chem.* **2015**, *7*, 19.
[2] M. S. Islam, C. A. Fisher, *Chem. Soc. Rev.* **2014**, *43*, 185.
[3] J. Peters, D. Buchholz, S. Passerini, M. Weil, *Energy Environ. Sci.* **2016**, *9*, 1744.
[4] C. Niu, J. Meng, X. Wang, C. Han, M. Yan, K. Zhao, X. Xu, W. Ren, Y. Zhao, L. Xu, *Nat. Commun.* **2015**, *6*, 7402.

[5] L. Mai, X. Tian, X. Xu, L. Chang, L. Xu, *Chem. Rev.* **2014**, *114*, 11828.
[6] J. B. Goodenough, K. S. Park, *J. Am. Chem. Soc.* **2013**, *135*, 1167.
[7] V. Palomares, M. Casas-Cabanas, E. Castillo-Martínez, M. H. Han, T. Rojo, *Energy Environ. Sci.* **2013**, *6*, 2312.
[8] W. Ren, Z. Zheng, Y. Luo, W. Chen, C. Niu, K. Zhao, M. Yan, L. Zhang, J. Meng, L. Mai, *J. Mater. Chem. A* **2015**, *3*, 19850.
[9] S. W. Kim, D. H. Seo, X. Ma, G. Ceder, K. Kang, *Adv. Energy Mater.* **2012**, *2*, 710.
[10] N. Yabuuchi, K. Kubota, M. Dahbi, S. Komaba, *Chem. Rev.* **2014**, *114*, 11636.
[11] C. Masquelier, L. Croguennec, *Chem. Rev.* **2013**, *113*, 6552.
[12] X. Wang, Y. Chen, OG. Schmidt, C. Yan, *Chem. Soc. Rev.* **2015**, *45*, 1308.
[13] L. W. Shacklette, J. E. Toth, R. L. Elsenbaumer, U.S. Patent 4,695,521 **1987**.
[14] T. Shishikura, M. Takeuchi, Y. Murakoshi, H. Konuma, M. Kameyama, U.S. Patent 5,051,325 **1991**.
[15] B. Dunn, H. Kamath, J. M. Tarascon, *Science* **2011**, *334*, 928.
[16] X. Xiang, K. Zhang, J. Chen, *Adv. Mater.* **2015**, *27*, 5343.
[17] H. Kang, Y. Liu, K. Cao, Y. Zhao, L. Jiao, Y. Wang, H. Yuan, *J. Mater. Chem. A* **2015**, *3*, 17899.
[18] J. Y. Hwang, S. M. Oh, S. T. Myung, K. Y. Chung, I. Belharouak, Y. K. Sun, *Nat. Commun.* **2015**, *6*, 6865.
[19] B. Zhang, R. Dugas, G. Rousse, P. Rozier, A. M. Abakumov, J.-M. Tarascon, *Nat. Commun.* **2016**, *7*, 10308.
[20] J. Ni, S. Fu, C. Wu, Y. Zhao, J. Maier, Y. Yu, L. Li, *Adv. Energy Mater.* **2016**, *28*, 2259.
[21] L. Liang, Y. Xu, C. Wang, L. Wen, Y. Fang, Y. Mi, M. Zhou, H. Zhao, Y. Lei, *Energy Environ. Sci.* **2015**, *8*, 2954.
[22] Z. Li, D. Young, K. Xiang, W. C. Carter, Y.-M. Chiang, *Adv. Energy Mater.* **2013**, *3*, 290.
[23] D. Kundu, E. Talaie, V. Duffort, L. F. Nazar, *Angew. Chem.* **2015**, *54*, 3431.
[24] L. P. Wang, L. Yu, X. Wang, M. Srinivasan, Z. J. Xu, *J. Mater. Chem. A* **2015**, *3*, 9353.
[25] C. Fang, Y. Huang, W. Zhang, J. Han, Z. Deng, Y. Cao, H. Yang, *Adv. Energy Mater.* **2015**, *6*, 1501727.
[26] M. H. Han, E. Gonzalo, G. Singh, T. Rojo, *Energy Environ. Sci.* **2015**, *8*, 81.
[27] R. J. Clément, P. G. Bruce, C. P. Grey, *J. Electrochem. Soc.* **2015**, *162*, A2589.
[28] H. Kim, H. Kim, Z. Ding, M. H. Lee, K. Lim, G. Yoon, K. Kang, *Adv. Energy Mater.* **2016**, *6*, 1600943.
[29] M. Dahbi, N. Yabuuchi, K. Kubota, K. Tokiwa, S. Komaba, *Phys. Chem. Chem. Phys.* **2014**, *16*, 15007.
[30] A. Ponrouch, D. Monti, A. Boschin, B. Steen, P. Johansson, M. R. Palacín, *J. Mater. Chem. A* **2015**, *3*, 22.
[31] V. Palomares, P. Serras, I. Villaluenga, K. B. Hueso, J. Carretero-González, T. Rojo, *Energy Environ. Sci.* **2012**, *5*, 5884.
[32] K. Kubota, S. Komaba, *J. Electrochem. Soc.* **2015**, *162*, A2538.
[33] C. Liu, R. Massé, X. Nan, G. Cao, *Energy Storage Mater.* **2016**, *4*, 15.
[34] S. Y. Hong, Y. Kim, Y. Park, A. Choi, N.-S. Choi, K. T. Lee, *Energy Environ. Sci.* **2013**, *6*, 2067.
[35] A. W. Golubkov, D. Fuchs, J. Wagner, H. Wiltsche, C. Stangl, G. Fauler, G. Voitic, A. Thaler, V. Hacker, *RSC Adv.* **2014**, *4*, 3633.
[36] U. Kasavajjula, C. Wang, A. J. Appleby, *J. Power Sources* **2007**, *163*, 1003.
[37] M. Yoshio, T. Tsumura, N. Dimov, *J. Power Sources* **2005**, *146*, 10.
[38] R. Dugas, B. Zhang, P. Rozier, J. M. Tarascon, *J. Electrochem. Soc.* **2016**, *163*, A867.
[39] R. Gupta, A. Manthiram, *J. Solid State Chem.* **1996**, *121*, 483.
[40] C. Delmas, C. Fouassier, P. Hagenmuller, *Physica B+C* **1980**, *99*, 81.
[41] R. Berthelot, D. Carlier, C. Delmas, *Nat. Mater.* **2011**, *10*, 74.
[42] J. Ding, Y. Zhou, Q. Sun, X. Yu, X. Yang, Z. Fu, *Electrochim. Acta* **2013**, *87*, 388.
[43] A. K. Rai, L. T. Anh, J. Gim, V. Mathew, J. Kim, *Ceram. Int.* **2013**, *40*, 2411.
[44] I. Hasa, X. Dou, D. Buchholz, Y. Shao-Horn, J. Hassoun, S. Passerini, B. Scrosati, *J. Power Sources* **2016**, *310*, 26.
[45] N. Yabuuchi, M. Kajiyama, J. Iwatate, H. Nishikawa, S. Hitomi, R. Okuyama, R. Usui, Y. Yamada, S. Komaba, *Nat. Mater.* **2012**, *11*, 512.
[46] D. Su, C. Wang, H. J. Ahn, D. G. Wang, *Chem. - Eur. J.* **2013**, *19*, 10884.
[47] H. Kim, G. Yoon, I. Park, K. Y. Park, B. Lee, J. Kim, Y. U. Park, S. K. Jung, H. D. Lim, D. Ahn, S. Lee, K. Kang, *Energy Environ. Sci.* **2015**, *8*, 3325.
[48] Y. Cao, L. Xiao, W. Wang, D. Choi, Z. Nie, J. Yu, L. V. Saraf, Z. Yang, J. Liu, *Adv. Mater.* **2011**, *23*, 3155.
[49] J. Braconnier, C. Delmas, P. Hagenmuller, *Mater. Res. Bull.* **1982**, *17*, 993.
[50] S. Komaba, C. Takei, T. Nakayama, A. Ogata, N. Yabuuchi, *Electrochem. Commun.* **2010**, *12*, 355.
[51] S. T. Myung, S. Komaba, N. Hirosaki, N. Kumagai, *Electrochem. Commun.* **2002**, *4*, 397.
[52] C. Y. Yu, J. S. Park, H. G. Jung, K. Y. Chung, D. Aurbach, Y. K. Sun, S.-. Myung, *Energy Environ. Sci.* **2015**, *8*, 2019.
[53] S. Hartung, N. Bucher, V. S. Nair, C. Y. Ling, Y. Wang, H. E. Hoster, M. Srinivasan, *ChemPhysChem.* **2014**, *15*, 2121.
[54] K. Park, B. C. Yu, J. B. Goodenough, *Chem. Mater.* **2015**, *27*, 6682.
[55] Y. Dong, S. Li, K. Zhao, C. Han, W. Chen, B. Wang, L. Wang, B. Xu, Q. Wei, L. Zhang, X. Xu, L. Mai, *Energy Environ. Sci.* **2015**, *8*, 1267.
[56] Y. Lei, X. Li, L. Liu, G. Ceder, *Chem. Mater.* **2014**, *26*, 5288.
[57] J. Billaud, R. J. Clément, A. R. Armstrong, J. Canales-Vázquez, P. Rozier, C. P. Grey, P. G. Bruce, *J. Am. Chem. Soc.* **2014**, *136*, 17243.
[58] J. Zhao, L. Zhao, K. Chihara, S. Okada, J. I. Yamaki, S. Matsumoto, S. Kuze, K. Nakane, *J. Electrochem. Soc.* **2013**, *160*, A3077.
[59] Y. Wang, R. Xiao, Y. S. Hu, M. Avdeev, L. Chen, *Nat. Commun.* **2015**, *6*, 6954.
[60] S. Guo, H. Yu, P. Liu, Y. Ren, T. Zhang, M. Chen, M. Ishida, H. Zhou, *Energy Environ. Sci.* **2015**, *8*, 1237.
[61] D. Yuan, X. Liang, L. Wu, Y. Cao, X. Ai, J. Feng, H. Yang, *Adv. Mater.* **2014**, *26*, 6301.
[62] E. de la Llave, V. Borgel, K. J. Park, J. Y. Hwang, Y. K. Sun, P. Hartmann, F. F. Chesneau, D. Aurbach, *ACS Appl. Mater. Inter.* **2016**, *8*, 1867.
[63] S. M. Oh, S. T. Myung, M. W. Jang, B. Scrosati, J. Hassoun, Y. K. Sun, *Phys. Chem. Chem. Phys.* **2013**, *15*, 3827.
[64] S. G, P. L, H. Yu, Y. Zhu, M. Chen, M. Ishida, H. Zhou, *Angew. Chem.* **2015**, *54*, 5894.
[65] J. Xu, D. H. Lee, R. J. Clément, X. Yu, M. Leskes, A. J. Pell, G. Pintacuda, X. Q. Yang, C. P. Grey, Y. S. Meng, *Chem. Mater.* **2014**, *26*, 1260.
[66] S. Guo, P. Liu, Y. Sun, K. Zhu, J. Yi, M. Chen, M. Ishida, H. Zhou, *Angew. Chem.* **2015**, *54*, 11701.
[67] L. Mu, S. Xu, Y. Li, Y. S. Hu, H. Li, L. Chen, X. Huang, *Adv. Mater.* **2015**, *27*, 6928.
[68] H. Wang, X.-Z. Liao, Y. Yang, X. Yan, Y.-S. He, Z.-F. Ma, *J. Electrochem. Soc.* **2016**, *163*, A565.
[69] D. Kim, E. Lee, M. Slater, W. Lu, S. Rood, C. S. Johnson, *Electrochem. Commun.* **2012**, *18*, 66.
[70] S. M. Oh, S. T. Myung, C. S. Yoon, J. Lu, J. Hassoun, B. Scrosati, K. Amine, Y. K. Sun, *Nano Lett.* **2014**, *14*, 1620.
[71] Y. Li, Z. Yang, S. Xu, L. Mu, L. Gu, Y.-S. Hu, H. Li, L. Chen, *Adv. Sci.* **2015**, *2*, 1500031.
[72] X. Qi, Y. Wang, L. Jiang, L. Mu, C. Zhao, L. Liu, Y. S. Hu, L. Chen, X. Huang, *Part. Part. Syst. Charact.* **2015**, *33*, 538.

[73] M. Matsui, F. Mizukoshi, N. Imanishi, *J. Power Sources* **2015**, *280*, 205.
[74] J. Billaud, G. Singh, A. R. Armstrong, E. Gonzalo, V. Roddatis, M. Armand, T. Rojo, P. G. Bruce, *Energy Environ. Sci.* **2014**, *7*, 1387.
[75] R. Kataoka, T. Mukai, A. Yoshizawa, T. Sakai, *J. Electrochem. Soc.* **2013**, *160*, A933.
[76] Z. Jian, H. Yu, H. Zhou, *Electrochem. Commun.* **2013**, *34*, 215.
[77] H. Liu, J. Xu, C. Ma, Y. S. Meng, *Chem. Commun.* **2015**, *51*, 4693.
[78] D. Kim, S. H. Kang, M. Slater, S. Rood, J. T. Vaughey, N. Karan, M. Balasubramanian, C. S. Johnson, *Adv. Energy Mater.* **2011**, *1*, 333.
[79] J. Xu, D. H. Lee, R. l. J. Clément, X. Yu, M. Leskes, A. J. Pell, G. Pintacuda, X.-Q. Yang, C. P. Grey, Y. S. Meng, *Chem. Mater.* **2014**, *26*, 1260.
[80] S.-M. Oh, S.-T. Myung, J. Y. Hwang, B. Scrosati, K. Amine, Y.-K. Sun, *Chem. Mater.* **2014**, *26*, 6165.
[81] A. Yamada, S. C. Chung, K. Hinokuma, *ChemInform* **2001**, *32*, 17.
[82] Z. Chen, J. R. Dahn, *J. Electrochem. Soc.* **2001**, *149*, A1184.
[83] Y. Zhu, Y. Xu, Y. Liu, C. Luo, C. Wang, *Nanoscale* **2012**, *5*, 780.
[84] M. Galceran, D. Saurel, B. Acebedo, V. V. Roddatis, E. Martin, T. Rojo, M. Casas-Cabanas, *Phys. Chem. Chem. Phys.* **2014**, *16*, 8837.
[85] J. Kim, D. H. Seo, H. Kim, I. Park, J. K. Yoo, S. K. Jung, Y. U. Park, W. A. G. Iii, K. Kang, *Energy Environ. Sci.* **2015**, *8*, 540.
[86] J.-K. Kim, Y. J. Lim, H. Kim, G.-B. Cho, Y. Kim, *Energy Environ. Sci.* **2015**, *8*, 3589.
[87] K. Saravanan, C. W. Mason, A. Rudola, K. H. Wong, P. Balaya, *Adv. Energy Mater.* **2013**, *3*, 444.
[88] Y. Jiang, Z. Yang, W. Li, L. Zeng, F. Pan, M. Wang, X. Wei, G. Hu, L. Gu, Y. Yu, *Adv. Energy Mater.* **2015**, *5*, 1402104.
[89] X. Wang, C. Niu, J. Meng, P. Hu, X. Xu, X. Wei, L. Zhou, K. Zhao, W. Luo, M. Yan, *Adv. Energy Mater.* **2015**, *5*, 939.
[90] H. Gao, W. Zhou, K. Park, J. B. Goodenough, *Adv. Energy Mater.* **2016**, *6*, 1502130.
[91] Z. Jian, W. Han, X. Lu, H. Yang, Y. S. Hu, J. Zhou, Z. Zhou, J. Li, W. Chen, D. Chen, *Adv. Energy Mater.* **2013**, *3*, 156.
[92] S. Li, Y. Dong, L. Xu, X. Xu, L. He, L. Mai, *Adv. Mater.* **2014**, *26*, 3545.
[93] C. Zhu, P. Kopold, P. A. van Aken, J. Maier, Y. Yu, *Adv. Mater.* **2016**, *28*, 2409.
[94] Y. Zhang, H. Zhao, Y. Du, *J. Mater. Chem. A* **2016**, *4*, 7155.
[95] Y. Fang, L. Xiao, J. Qian, Y. Cao, X. Ai, Y. Huang, H. Yang, *Adv. Energy Mater.* **2016**, *6*, 1502197.
[96] W. Ren, Z. Zheng, C. Xu, C. Niu, Q. Wei, Q. An, K. Zhao, M. Yan, M. Qin, L. Mai, *Nano Energy* **2016**, *25*, 145.
[97] Z. Yuan, L. Si, X. Zhu, *J. Mater. Chem. A* **2015**, *3*, 23403.
[98] W. Ren, X. Yao, C. Niu, Z. Zheng, K. Zhao, Q. An, Q. Wei, M. Yan, L. Zhang, L. Mai, *Nano Energy* **2016**, *28*, 216.
[99] G. He, W. H. Kan, A. Manthiram, *Chem. Mater.* **2016**, *28*, 682.
[100] H. Li, L. Peng, Y. Zhu, D. Chen, X. Zhang, G. Yu, *Energy Environ. Sci.* **2016**, *9*, 3399.
[101] L. Mu, L. Ben, Y. S. Hu, H. Li, L. Chen, X. Huang, *J. Mater. Chem. A* **2016**, *4*, 7141.
[102] Z. Liu, Y. Y. Hu, M. T. Dunstan, H. Huo, X. Hao, H. Zou, G. Zhong, Y. Yang, C. P. Grey, *Chem. Mater.* **2014**, *26*, 2513.
[103] A. Ponrouch, R. Dedryvère, D. Monti, A. E. Demet, J. M. Ateba Mba, L. Croguennec, C. Masquelier, P. Johansson, M. R. Palacín, *Energy Environ. Sci.* **2013**, *6*, 2361.
[104] K. Chihara, A. Kitajou, I. D. Gocheva, S. Okada, J.-I. Yamaki, *J. Power Sources* **2013**, *227*, 80.
[105] J. Barker, M. Saidi, J. Swoyer, *Electrochem. Solid-State Lett.* **2003**, *6*, A1.
[106] P. Barpanda, S. I. Nishimura, A. Yamada, *Adv. Energy Mater.* **2012**, *2*, 841.
[107] M. Nose, H. Nakayama, K. Nobuhara, H. Yamaguchi, S. Nakanishi, H. Iba, *J. Power Sources* **2013**, *234*, 175.
[108] Y. Niu, M. Xu, C. Cheng, S. Bao, J. Hou, S. Liu, F. Yi, H. He, C. M. Li, *J. Mater. Chem. A* **2015**, *3*, 17224.
[109] Y. You, X. L. Wu, Y. X. Yin, Y. G. Guo, *Energy Environ. Sci.* **2014**, *7*, 1643.
[110] Y. Lu, L. Wang, J. Cheng, J. B. Goodenough, *Chem. Commun.* **2012**, *48*, 6544.
[111] J. Song, L. Wang, Y. Lu, J. Liu, B. Guo, P. Xiao, J. J. Lee, X. Q. Yang, G. Henkelman, J. B. Goodenough, *J. Am. Chem. Soc.* **2015**, *137*, 2658.
[112] L. Wang, J. Song, R. Qiao, L. A. Wray, M. A. Hossain, Y. D. Chuang, W. Yang, Y. Lu, D. Evans, J. J. Lee, S. Vail, X. Zhao, M. Nishijima, S. Kakimoto, J. B. Goodenough, *J. Am. Chem. Soc.* **2015**, *137*, 2548.
[113] J. Qian, M. Zhou, Y. Cao, X. Ai, H. Yang, *Adv. Energy Mater.* **2012**, *2*, 410.
[114] D. Yang, J. Xu, X. Z. Liao, Y. S. He, H. Liu, Z. F. Ma, *Chem. Commun.* **2014**, *50*, 13377.
[115] M. Armand, J. M. Tarascon, *Nature* **2008**, *451*, 652.
[116] W. Xu, A. Read, P. K. Koech, D. Hu, C. Wang, J. Xiao, A. B. Padmaperuma, G. L. Graff, J. Liu, J. G. Zhang, *J. Mater. Chem.* **2012**, *22*, 4032.
[117] T. Suga, H. Ohshiro, S. Sugita, K. Oyaizu, H. Nishide, *Adv. Mater.* **2009**, *21*, 1627.
[118] S. Wang, L. Wang, Z. Zhu, Z. Hu, Q. Zhao, J. Chen, *Angew. Chem.* **2014**, *53*, 5892.
[119] H. Wang, P. Hu, J. Yang, G. Gong, L. Guo, X. Chen, *Adv. Mater.* **2015**, *27*, 2348.
[120] K. Chihara, N. Chujo, A. Kitajou, S. Okada, *Electrochim. Acta* **2013**, *110*, 240.
[121] L. Chen, W. Li, Y. Wang, C. Wang, Y. Xia, *RSC Adv.* **2014**, *4*, 25369.
[122] H. Banda, D. Damien, K. Nagarajan, M. Hariharan, M. M. Shaijumon, *J. Mater. Chem. A* **2015**, *3*, 10453.
[123] W. Deng, X. Liang, X. Wu, J. Qian, Y. Cao, X. Ai, J. Feng, H. Yang, *Sci. Rep.* **2013**, *3*, 2671.
[124] Y. Cao, L. Xiao, M. L. Sushko, W. Wang, B. Schwenzer, J. Xiao, Z. Nie, L. V. Saraf, Z. Yang, J. Liu, *Nano Lett.* **2012**, *12*, 3783.
[125] T. Yang, T. Qian, M. Wang, X. Shen, N. Xu, Z. Sun, C. Yan, *Adv. Mater.* **2016**, *28*, 539.
[126] F. Shen, W. Luo, J. Dai, Y. Yao, M. Zhu, E. Hitz, Y. Tang, Y. Chen, V. L. Sprenkle, X. Li, *Adv. Energy Mater.* **2016**, *6*, 1600377.
[127] Y. Li, Y. S. Hu, M. M. Titirici, L. Chen, X. Huang, *Adv. Energy Mater.* **2016**, *6*, 1600659.
[128] Y. Wen, K. He, Y. Zhu, F. Han, Y. Xu, I. Matsuda, Y. Ishii, J. Cumings, C. Wang, *Nat. Commun.* **2014**, *5*, 4033.
[129] B. Jache, P. Adelhelm, *Angew. Chem. Int. Ed.* **2014**, *53*, 10169.
[130] H. Kim, J. Hong, Y. U. Park, J. Kim, I. Hwang, K. Kang, *Adv. Funct. Mater.* **2015**, *25*, 534.
[131] P. Han, B. Zhang, C. Huang, L. Gu, H. Li, G. Cui, *Electrochem. Commun.* **2014**, *44*, 70.
[132] P. Han, X. Han, J. Yao, Z. Liu, X. Cao, G. Cui, *Electrochem. Commun.* **2015**, *61*, 84.
[133] Z. Zhu, F. Cheng, Z. Hu, Z. Niu, J. Chen, *J. Power Sources* **2015**, *293*, 626.
[134] D. Stevens, J. Dahn, *J. Electrochem. Soc.* **2000**, *147*, 1271.
[135] Z. Wang, L. Qie, L. Yuan, W. Zhang, X. Hu, Y. Huang, *Carbon* **2013**, *55*, 328.
[136] S. Komaba, W. Murata, T. Ishikawa, N. Yabuuchi, T. Ozeki, T. Nakayama, A. Ogata, K. Gotoh, K. Fujiwara, *Adv. Funct. Mater.* **2011**, *21*, 3859.
[137] R. Mukherjee, A. V. Thomas, D. Datta, E. Singh, J. Li, O. Eksik, V. B. Shenoy, N. Koratkar, *Nat. Commun.* **2014**, *5*, 3710.
[138] S. Komaba, W. Murata, T. Ishikawa, N. Yabuuchi, T. Ozeki, T. Nakayama, A. Ogata, K. Gotoh, K. Fujiwara, *Adv. Funct. Mater.* **2011**, *21*, 3859.
[139] C. Ding, T. Nohira, R. Hagiwara, A. Fukunaga, S. Sakai, K. Nitta, *Electrochim. Acta* **2015**, *176*, 344.

[140] B. Zhang, C. M. Ghimbeu, C. Laberty, C. Vix-Guterl, J. M. Tarascon, *Adv. Energy Mater.* **2016**, *6*, 1501588.
[141] Y. Li, S. Xu, X. Wu, J. Yu, Y. Wang, Y. S. Hu, H. Li, L. Chen, X. Huang, *J. Mater. Chem. A* **2015**, *3*, 71.
[142] Y. Li, Y. S. Hu, H. Li, L. Chen, X. Huang, *J. Mater. Chem. A* **2016**, *4*, 96.
[143] E. M. Lotfabad, J. Ding, K. Cui, A. Kohandehghan, W. P. Kalisvaart, M. Hazelton, D. Mitlin, *ACS Nano* **2014**, *8*, 7115.
[144] K. L. Hong, L. Qie, R. Zeng, Z. q. Yi, W. Zhang, D. Wang, W. Yin, C. Wu, Q. J. Fan, W. X. Zhang, *J. Mater. Chem. A* **2014**, *2*, 12733.
[145] L. Wu, D. Buchholz, C. Vaalma, G. A. Giffin, S. Passerini, *ChemElectroChem* **2016**, *3*, 292.
[146] L. Wu, X. Hu, J. Qian, F. Pei, F. Wu, R. Mao, X. Ai, H. Yang, Y. Cao, *Energy Environ. Sci.* **2014**, *7*, 323.
[147] V. L. Chevrier, G. Ceder, *J. Electrochem. Soc.* **2011**, *158*, A1011.
[148] A. Darwiche, C. Marino, M. T. Sougrati, B. Fraisse, L. Stievano, L. Monconduit, *J. Am. Chem. Soc.* **2012**, *134*, 20805.
[149] X. Xie, K. Kretschmer, J. Zhang, B. Sun, D. Su, G. Wang, *Nano Energy* **2015**, *13*, 208.
[150] Y. Liu, N. Zhang, L. Jiao, J. Chen, *Adv. Mater.* **2015**, *27*, 6702.
[151] W. Zhang, Y. Liu, C. Chen, Z. Li, Y. Huang, X. Hu, *Small* **2015**, *11*, 3822.
[152] J. Zhang, Y. X. Yin, Y. G. Guo, *ACS Appl. Mater. Inter.* **2015**, *7*, 27838.
[153] W. Li, S. L. Chou, J. Z. Wang, J. H. Kim, H. K. Liu, S. X. Dou, *Adv. Mater.* **2014**, *26*, 4037.
[154] M. Walter, S. Doswald, M. V. Kovalenko, *J. Mater. Chem. A* **2016**, *4*, 7053.
[155] W. Li, C. Hu, M. Zhou, H. Tao, K. Wang, S. Cheng, K. Jiang, *J. Power Sources* **2016**, *307*, 173.
[156] N. Wang, Z. Bai, Y. Qian, J. Yang, *Adv. Mater.* **2016**, *28*, 4126.
[157] A. Moretti, M. Secchiaroli, D. Buchholz, G. Giuli, R. Marassi, S. Passerini, *J. Electrochem. Soc.* **2015**, *162*, A2723.
[158] M. C. Lopez, M. J. Aragon, G. F. Ortiz, P. Lavela, R. Alcantara, J. L. Tirado, *Chem. Eur. J.* **2015**, *21*, 14879.
[159] M. N. Tahir, B. Oschmann, D. Buchholz, X. Dou, I. Lieberwirth, M. Panthöfer, W. Tremel, R. Zentel, S. Passerini, *Adv. Energy Mater.* **2016**, *6*, 1501489.
[160] L. Zhao, Y. S. Hu, H. Li, Z. Wang, L. Chen, *Adv. Mater.* **2011**, *23*, 1385.
[161] Y. Sun, L. Zhao, H. Pan, X. Lu, L. Gu, Y. S. Hu, H. Li, M. Armand, Y. Ikuhara, L. Chen, X. Huang, *Nat. Commun.* **2013**, *4*, 1870.
[162] H. Xiong, M. D. Slater, M. Balasubramanian, C. S. Johnson, T. Rajh, *J. Phys. Chem. Lett.* **2011**, *2*, 2560.
[163] A. Rudola, K. Saravanan, S. Devaraj, H. Gong, P. Balaya, *Chem. Commun.* **2013**, *49*, 7451.
[164] Y. Wang, X. Yu, S. Xu, J. Bai, R. Xiao, Y. S. Hu, H. Li, X. Q. Yang, L. Chen, X. Huang, *Nat. Commun.* **2013**, *4*, 2365.
[165] P. R. Kumar, Y. H. Jung, K. K. Bharathi, C. H. Lim, D. K. Kim, *Electrochim. Acta* **2014**, *146*, 503.
[166] H. Ye, Y. Wang, F. Zhao, W. Huang, N. Han, J. Zhou, M. Zeng, Y. Li, *J. Mater. Chem. A* **2016**, *4*, 1754.
[167] S. Hariharan, K. Saravanan, P. Balaya, *Electrochem. Commun.* **2013**, *31*, 5.
[168] Z. Hu, L. Wang, K. Zhang, J. Wang, F. Cheng, Z. Tao, J. Chen, *Angew. Chem.* **2014**, *126*, 13008.
[169] C. Wu, Y. Jiang, P. Kopold, P. A. van Aken, J. Maier, Y. Yu, *Adv. Mater.* **2016**, *28*, 7276.
[170] Z. Hu, Z. Zhu, F. Cheng, K. Zhang, J. Wang, C. Chen, J. Chen, *Energy Environ. Sci.* **2015**, *8*, 1309.
[171] K. Zhang, Z. Hu, X. Liu, Z. Tao, J. Chen, *Adv. Mater.* **2015**, *27*, 3305.
[172] S. Peng, X. Han, L. Li, Z. Zhu, F. Cheng, M. Srinivansan, S. Adams, S. Ramakrishna, *Small* **2016**, *12*, 1359.
[173] W. Sun, X. Rui, D. Yang, Z. Sun, B. Li, W. Zhang, Y. Zong, S. Madhavi, S. Dou, Q. Yan, *ACS Nano* **2015**, *9*, 11371.
[174] B. Qu, C. Ma, G. Ji, C. Xu, J. Xu, Y. S. Meng, T. Wang, J. Y. Lee, *Adv. Mater.* **2014**, *26*, 3854.
[175] D. Y. Yu, P. V. Prikhodchenko, C. W. Mason, S. K. Batabyal, J. Gun, S. Sladkevich, A. G. Medvedev, O. Lev, *Nat. Commun.* **2013**, *4*, 2922.
[176] Y. Liu, N. Zhang, H. Kang, M. Shang, L. Jiao, J. Chen, *Chem. Eur. J.* **2015**, *21*, 11878.
[177] Y. C. Lu, C. Ma, J. Alvarado, N. Dimov, Y. S. Meng, S. Okada, *J. Mater. Chem. A* **2015**, *3*, 16971.
[178] P. R. Kumar, Y. H. Jung, D. K. Kim, *RSC Adv.* **2015**, *5*, 79845.
[179] W. Sun, X. Rui, D. Zhang, Y. Jiang, Z. Sun, H. Liu, S. Dou, *J. Power Sources* **2016**, *309*, 135.
[180] A. Abouimrane, W. Weng, H. Eltayeb, Y. Cui, J. Niklas, O. Poluektov, K. Amine, *Energy Environ. Sci.* **2012**, *5*, 9632.
[181] X. Y. Wu, M. Y. Sun, Y. F. Shen, J. F. Qian, Y. L. Cao, X. P. Ai, H. X. Yang, *ChemSusChem* **2014**, *7*, 407.
[182] Z. Song, H. Zhan, Y. Zhou, *Angew. Chem. Int. Ed.* **2010**, *49*, 8444.
[183] N. Alias, A. A. Mohamad, *J. Power Sources* **2015**, *274*, 237.
[184] J. Yun, J. Pfisterer, A. S. Bandarenka, *Energy Environ. Sci.* **2016**, *9*, 955.
[185] K. Nakamoto, Y. Kano, A. Kitajou, S. Okada, *J. Power Sources* **2016**, *327*, 327.
[186] J. F. Whitacre, T. Wiley, S. Shanbhag, Y. Wenzhuo, A. Mohamed, S. E. Chun, E. Weber, D. Blackwood, E. Lynch-Bell, J. Gulakowski, *J. Power Sources* **2012**, *213*, 255.
[187] Y. Meng, Y. Yang, *Electrochem. Commun.* **2007**, *9*, 1428.
[188] C. Cao, Z. B. Li, X. L. Wang, X. B. Zhao, W. Q. Han, *Frontiers in Energy Research* **2014**, *2*, 25.
[189] M. C. López, G. F. Ortiz, E. M. Arroyo-de Dompablo, J. L. Tirado, *Inorg. Chem.* **2014**, *53*, 2310.
[190] D. Saikia, Y. H. Chen, Y. C. Pan, J. Fang, L. D. Tsai, G. T. Fey, H. M. Kao, *J. Mater. Chem.* **2011**, *21*, 10542.
[191] P. Barbosa, L. Rodrigues, M. Silva, M. Smith, A. Gonçalves, E. Fortunato, *J. Mater. Chem.* **2010**, *20*, 723.
[192] W. Li, J. R. Dahn, D. S. Wainwright, *Science* **1994**, *264*, 1115.
[193] J. Y. Luo, W. J. Cui, P. He, Y.-Y. Xia, *Nat. Chem.* **2010**, *2*, 760.
[194] L. Suo, O. Borodin, T. Gao, M. Olguin, J. Ho, X. Fan, C. Luo, C. Wang, K. Xu, *Science* **2015**, *350*, 938.
[195] C. Mi, X. Zhang, H. Li, *J. Electro. Chem.* **2007**, *602*, 245.
[196] S. I. Park, I. Gocheva, S. Okada, J.-I. Yamaki, *J. Electrochem. Soc.* **2011**, *158*, A1067.
[197] J. F. Whitacre, A. Tevar, S. Sharma, *Electrochem. Commun.* **2010**, *12*, 463.
[198] B. Zhao, B. Lin, S. Zhang, C. Deng, *Nanoscale* **2015**, *7*, 18552.
[199] W. Wu, J. Yan, A. Wise, A. Rutt, J. F. Whitacre, *J. Electrochem. Soc.* **2014**, *161*, A561.
[200] W. Wu, S. Shabhag, J. Chang, A. Rutt, J. F. Whitacre, *J. Electrochem. Soc.* **2015**, *162*, A803.
[201] P. R. Kumar, Y. H. Jung, B. Moorthy, D. K. Kim, *J. Electrochem. Soc.* **2016**, *163*, A1484.
[202] Z. Li, D. B. Ravnsbæk, K. Xiang, Y. M. Chiang, *Electrochem. Commun.* **2014**, *44*, 12.
[203] Y. Liu, Y. Qiao, W. Zhang, H. Xu, Z. Li, Y. Shen, L. Yuan, X. Hu, X. Dai, Y. Huang, *Nano Energy* **2014**, *5*, 97.
[204] Z. Hou, X. Li, J. Liang, Y. Zhu, Y. Qian, *J. Mater. Chem. A* **2015**, *3*, 1400.
[205] Y. Wang, L. Mu, J. Liu, Z. Yang, X. Yu, L. Gu, Y. S. Hu, H. Li, X. Q. Yang, L. Chen, X. Huang, *Adv. Energy Mater.* **2015**, *5*, 1501005.
[206] X. Y. Wu, M. Y. Sun, Y. F. Shen, J. F. Qian, Y. L. Cao, X. P. Ai, H. X. Yang, *ChemSusChem* **2014**, *7*, 407.
[207] X. Wu, Y. Cao, X. Ai, J. Qian, H. Yang, *Electrochem. Commun.* **2013**, *31*, 145.
[208] M. Pasta, C. D. Wessells, N. Liu, J. Nelson, M. T. McDowell, R. A. Huggins, M. F. Toney, Y. Cui, *Nat. Commun.* **2014**, *5*, 3007.
[209] P. R. Kumar, Y. H. Jung, C. H. Lim, D. K. Kim, *J. Mater. Chem. A* **2015**, *3*, 6271.

[210] A. J. Fernández-Ropero, D. Saurel, B. Acebedo, T. Rojo, M. Casas-Cabanas, *J. Power Sources* **2015**, *291*, 40.
[211] Y. Zhong, X. H. Xia, J. Zhan, X. Wang, J. Tu, *J. Mater. Chem. A* **2016**, *4*, 18717.
[212] I. Hasa, S. Passerini, J. Hassoun, *RSC Adv.* **2015**, *5*, 48928.
[213] I. Hasa, S. Passerini, J. Hassoun, *J. Power Sources* **2016**, *303*, 203.
[214] S. Xu, Y. Wang, L. Ben, Y. Lyu, N. Song, Z. Yang, Y. Li, L. Mu, H.-T. Yang, L. Gu, Y.-S. Hu, H. Li, Z.-H. Cheng, L. Chen, X. Huang, *Adv. Energy Mater.* **2015**, *5*, 1501156.
[215] I. Hasa, J. Hassoun, Y.-K. Sun, B. Scrosati, *Chem. Phys. Phys. Chem.* **2014**, *15*, 2152.
[216] G. L. Xu, Z. Chen, G. M. Zhong, Y. Liu, Y. Yang, T. Ma, Y. Ren, X. Zuo, X. H. Wu, X. Zhang, K. Amine, *Nano Lett.* **2016**, *16*, 3955.
[217] M. Fan, Y. Chen, Y. Xie, T. Yang, X. Shen, N. Xu, H. Yu, C. Yan, *Adv. Funct. Mater.* **2016**, *26*, 5019.
[218] X. Zhang, Z. Hou, X. Li, J. Liang, Y. Zhu, Y. Qian, *J. Mater. Chem. A* **2016**, *4*, 856.
[219] Y. Liu, Y. Qiao, X. Lou, X. Zhang, W. Zhang, Y. Huang, *ACS Appl. Mater. Inter.* **2016**, *8*, 14564.
[220] Y. Liu, Y. Qiao, W. Zhang, H. Wang, K. Chen, H. Zhu, Z. Li, Y. Huang, *J. Mater. Chem. A* **2015**, *3*, 7780.
[221] X. Wu, M. Sun, S. Guo, J. Qian, Y. Liu, Y. Cao, X. Ai, H. Yang, *ChemNanoMat* **2015**, *1*, 188.
[222] D. J. Kim, Y. H. Jung, K. K. Bharathi, S. H. Je, D. K. Kim, A. Coskun, J. W. Choi, *Adv. Energy Mater.* **2014**, *4*, 3412.
[223] M. Vujković, S. Mentus, *J. Power Sources* **2016**, *325*, 185.
[224] Q. Zhang, C. Liao, T. Zhai, H. Li, *Electrochim. Acta* **2016**, *196*, 470.
[225] W. Wu, A. Mohamed, J. F. Whitacre, *J. Electrochem. Soc.* **2013**, *160*, A497.
[226] Y. Liu, B. H. Zhang, S. Y. Xiao, L. L. Liu, Z. B. Wen, Y. P. Wu, *Electrochim. Acta* **2014**, *116*, 512.
[227] C. Deng, S. Zhang, Z. Dong, Y. Shang, *Nano Energy* **2014**, *4*, 49.
[228] H. Qin, Z. P. Song, H. Zhan, Y. H. Zhou, *J. Power Sources* **2014**, *249*, 367.

Received: December 18, 2016
Revised: February 19, 2017
Published online:

